

# REPORT 1157

## ANALYTICAL DERIVATION AND EXPERIMENTAL EVALUATION OF SHORT-BEARING APPROXIMATION FOR FULL JOURNAL BEARINGS<sup>1</sup>

By GEORGE B. DUBoIS and FRED W. OCVIRK

### SUMMARY

An approximate analytical solution including the effect of end leakage from the oil film of short plain bearings is presented because of the importance of endwise flow in sleeve bearings of the short lengths commonly used. The analytical approximation is supported by experimental data, resulting in charts which facilitate analysis of short plain bearings. The analytical approximation includes the endwise flow and that part of the circumferential flow which is related to surface velocity and film thickness but neglects the effect of film pressure on the circumferential flow. In practical use, this approximation applies best to bearings having a length-diameter ratio up to 1, and the effects of elastic deflection, inlet oil pressure, and changes of clearance with temperature minimize the relative importance of the neglected term. The analytical approximation was found to be an extension of a little-known pressure-distribution function originally proposed by Michell and Cardullo.

The experimental data on a 1½-inch shaft at speeds from 500 to 6,000 rpm and bearing loads up to 900 pounds per square inch are in useful agreement with the analytical curves for length-diameter ratios of ¼, ½, and 1. Single lines applying to  $l/d$  ratios up to 1 are obtained by using basic nondimensional quantities derived from the theoretical analysis. The reciprocal of the load number is the Sommerfeld number times the square of the length-diameter ratio. The friction ratio enables the friction to be estimated directly from the Petroff friction calculated at no load, avoiding the use of a friction coefficient. The oil flow factor reduces oil flow to a single line when plotted against an empirical modification of the load number. Methods are also discussed for approximating a maximum bearing temperature for pressure-lubricated bearings and for evaluating the effect of deflection or misalignment on the eccentricity ratio at the ends of a bearing.

### INTRODUCTION

The end leakage of oil flow has a predominant effect on narrow plain bearings, and an approximate solution including end-leakage effects would be useful. The following analytical and experimental investigation of such a solution was conducted at the School of Mechanical Engineering of Cornell University, Ithaca, New York, under the sponsorship and with the financial aid of the National Advisory Committee for Aeronautics.

Most investigators have based their functions on exact or approximate mathematical solutions of Reynolds' equation (ref. 1):

$$\frac{\partial}{\partial x} \left( h^3 \frac{\partial p}{\partial x} \right) + \frac{\partial}{\partial z} \left( h^3 \frac{\partial p}{\partial z} \right) = 6\mu U \frac{\partial h}{\partial x} \quad (1)$$

Kingsbury (ref. 2) determined the pressure distribution in the oil film of finite journal bearings satisfying equation (1) by an experimental electrical analogy. Christopherson (ref. 3) determined the film pressure in journal bearings of finite length by utilizing the mathematical method of "relaxation." Cameron and Wood (ref. 4) have extended the work of Christopherson to show the effect of length-diameter ratio on eccentricity ratio, attitude angle, and friction coefficient. In all cases, these solutions are given to express natural phenomena in the oil film on the basis of Reynolds' assumptions regarding lubrication, the most important assumption being that certain terms in the generalized Navier-Stokes equations (refs. 5 and 6) for flow in a viscous fluid may be neglected.

Solutions of Reynolds' equation, often termed approximate solutions, have been realized by considering either the second term or the first term of the left side of equation (1) equal to zero. Such solutions for pressure distribution give considerably simplified mathematical relationships among the variables. They are exact solutions in the sense that they satisfy equation (1) for the case of a bearing of infinite axial length on the one hand and for the infinitely short bearing on the other hand. However, they are regarded as approximate solutions when used to determine the pressure distribution in bearings of finite length.

Sommerfeld (ref. 7) and Harrison (ref. 8) presented a solution for journal bearings by assuming  $\partial p / \partial z = 0$ , thus eliminating the second of the left-hand terms of equation (1). Such an assumption states that there is no endwise flow as in the case of an infinitely long bearing.

Michell (ref. 9) suggested a solution for the journal bearing by dropping the first of the left-hand terms in Reynolds' equation. Cardullo (ref. 10) presented this solution as giving the pressure distribution in journal bearings of finite lengths usually found in engineering practice.

Because the Michell-Cardullo solution neglects the first of the left-hand terms in equation (1), it has been regarded as limited to bearings of infinitely short length. However, as indicated in the detailed treatment of this report, this assumption includes endwise flow and that part of the circumferential flow which is proportional to journal surface

<sup>1</sup> Incorporates most of information contained in NACA TN 2808, "Short-Bearing Approximation for Full Journal Bearings" by F. W. Ocvirk, 1952, and NACA TN 2809, "Experimental Investigation of Eccentricity Ratio, Friction, and Oil Flow of Short Journal Bearings" by G. B. DuBois and F. W. Ocvirk, 1952.

velocity and varying film thickness but neglects the effect of oil film pressure on the circumferential flow.

Experimental measurements of pressure distribution in finite journal bearings were obtained by McKee and McKee (ref. 11) sometime after the mathematical treatments of Michell and Cardullo were published and discussed. On comparison, it was shown that the theoretical Sommerfeld-Harrison distribution was not in agreement with the experimental data. Bradford and Grunder (ref. 12), after conducting experiments, also demonstrated that the Harrison theory did not agree for finite cases. Almost no effort was made to compare the Michell-Cardullo theory with the experiments although a comment was made by Hersey in reference 11 that Rouse had found the Michell-Cardullo theory to be in better agreement with experiment than was the Sommerfeld-Harrison theory.

This report extends the short-bearing pressure-distribution function of Michell and Cardullo to give equations for the various bearing characteristics. This short-bearing approximation makes available formulas relating eccentricity ratio to applied load, attitude angle, angular position of peak film pressure, friction, required oil flow, and the ratio of peak film pressure to unit pressure on projected area. Basic nondimensional quantities called the load number, the capacity number, the friction ratio, and the oil flow factor are derived which simplify the prediction of short-bearing performance.

Experimental oil film pressure data obtained by McKee and McKee (ref. 11) and DuBois, Mabie, and Ocvirk (ref. 13) indicate that the short-bearing pressure-distribution function is in reasonable agreement with natural phenomena for bearings having a length-diameter ratio near 1. This agreement motivated the experimental program of this report to provide bearing-performance data for comparison with the analytical curves from the short-bearing approximation.

### SYMBOLS

$C_n$	capacity number, $S\left(\frac{l}{d}\right)^2 = \frac{\mu N'}{p'} \left(\frac{d}{c_d}\right)^2 \left(\frac{l}{d}\right)^2$
$C_{p_o}$	inlet pressure capacity number, $\frac{\mu N'}{p_o} \left(\frac{d}{c_d}\right)^2 \left(\frac{l}{d}\right)^2$
$C_1, C_2$	constants of integration
$1/C_n$	load number
$c_d$	diametral clearance, $2c_r$ , in.
$c_d/d$	diametral clearance ratio
$c_r$	radial clearance, in.
$c_r/r$	radial clearance ratio
$d$	bearing diameter, in.
$e$	eccentricity of journal and bearing axes, in.
$F$	circumferential bearing friction force under load, lb
$F/F_o$	friction ratio
$F_c$	friction calibration factor, in-lb/in. mercury
$F_o$	circumferential bearing friction force at zero load, lb, $2\pi^2 \mu N' l d (d/c_d)$
$f$	friction coefficient, $F/P$

$f_s$	friction variable, $f \left(\frac{d}{c_d}\right) \left(\frac{l}{d}\right)^2$
$h$	local fluid film thickness, in.
$h_{min}$	fluid film thickness at closest approach, $c_r(1-n)$ , in.
$k$	peak-pressure ratio, $p_{max}/p'$
$l$	bearing length, in.
$l/d$	length-diameter ratio
$M_s$	friction torque, in-lb
$m$	integer
$N$	journal speed, rpm
$N'$	journal speed, rps
$n$	eccentricity ratio or attitude, $e/c_r$
$n_h$	horizontal component of eccentricity ratio
$n_v$	vertical component of eccentricity ratio
$P$	applied central load, lb
$P_x, P_y$	components of applied load parallel and normal to line of centers of journal and bearing, lb
$p$	local fluid film pressure, lb/sq in.
$p_{max}$	peak pressure in fluid film, lb/sq in.
$p_o$	oil pressure at inlet to bearing, lb/sq in.
$p_s$	pressure at $\theta=0$ and $\pi$ in theory of bearing without endwise flow, lb/sq in.
$p'$	unit pressure on projected area, lb/sq in.
$Q$	rate of total oil flow from bearing, in. <sup>3</sup> /sec
$Q_r$	rate of fluid flow required for converging oil film, in. <sup>3</sup> /sec
$Q'$	rate of oil flow, lb/min
$q$	oil flow factor, $Q/Q_r = Q/\pi d l c_d \frac{N'}{2} n = q_r/n$
$q_r$	required oil flow number, $Q_r/\pi d l c_d \frac{N'}{2}$
$q_x, q_z$	flow per unit time in $x$ - and $z$ -directions, in. <sup>3</sup> /sec
$r$	bearing radius, in.
$S$	Sommerfeld number, $\frac{\mu N'}{p'} \left(\frac{d}{c_d}\right)^2$
$T$	temperature, °F
$U$	surface speed of journal, in./sec
$u, v, w$	local fluid film velocities in $x$ -, $y$ -, and $z$ -directions, in./sec
$x, y, z$	coordinates
$\alpha$	angle measured from load line to location of peak film pressure, deg
$\theta$	angle measured from maximum film thickness
$\theta_{max}$	angle measured from location of maximum film thickness to location of peak film pressure, deg
$\mu$	absolute viscosity of fluid, reyns or centipoises/( $6.9 \times 10^6$ )
$\tau_x, \tau_z$	fluid shearing stress in $x$ - and $z$ -directions, lb/sq in.
$\phi$	attitude angle, angle between load line and line of centers of journal and bearing, deg

### ANALYTICAL DETERMINATION OF PRESSURE DISTRIBUTION IN SHORT JOURNAL BEARINGS

The early portion of the following analysis embodies the assumptions and analytical reasoning employed by Reynolds (ref. 1) to yield equation (1).

## ANALYSIS FOLLOWING REYNOLDS' METHOD

When acted upon by a normal central load, the rotating journal is made to displace with respect to the stationary bearing such that the element of fluid  $dx$ ,  $dy$ , and  $dz$  of figure 1 moves in a converging film of oil. Because the fluid is viscous, the rotating journal causes the element to flow into the wedge at a circumferential velocity  $u$ ; since the oil film is of finite extent in the axial direction of the bearing, the element has a velocity  $w$  in the endwise direction.

Both bearing and journal are of length  $l$  and diameter  $d$  or radius  $r$ . The journal rotates at a constant angular velocity having a surface velocity of  $U$  with respect to the stationary bearing surface. Because the centers of the bearing  $O$  and the journal  $O'$  are displaced by an amount  $e$ , the oil film will be of variable thickness  $h$ . It is assumed that the circumferential dimension of the film may be unwrapped such that the fluid is essentially moving between surfaces, one of which may be considered a plane. The coordinates  $x$ ,  $y$ , and  $z$  are chosen as shown in figure 1 such that the  $x$ -direction is circumferential, the  $y$ -direction is radial, and the  $z$ -direction is measured from the center of the bearing parallel to the bearing and journal axes.

Figure 2 shows the forces which are assumed to act on the fluid element in laminar flow at an arbitrary location in the converging oil film. In both  $x$ - and  $z$ -directions it is assumed that shearing stresses  $\tau_x$  and  $\tau_z$  and normal pressures  $p$  are acting as shown. In the  $x$ -direction, for example, two shearing vectors and two normal vectors are assumed; in

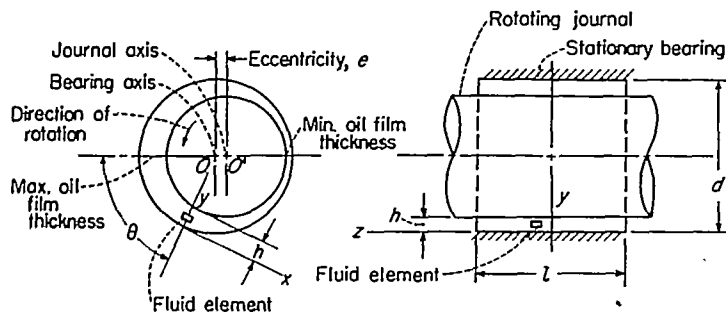
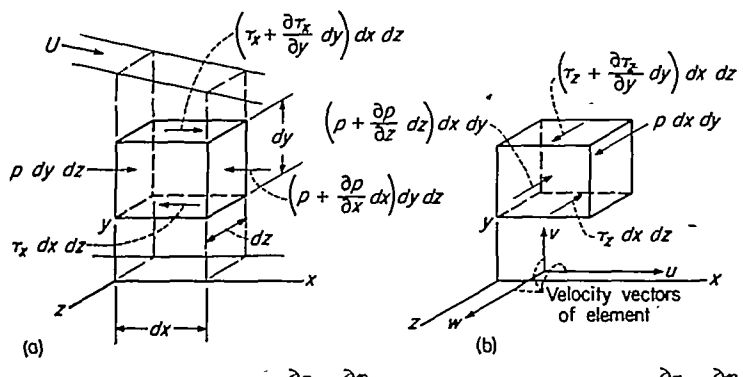


FIGURE 1.—Fluid element in converging oil film of cylindrical bearing with endwise flow.



(a) In  $x$ -direction where  $\frac{\partial \tau_x}{\partial y} = \frac{\partial p}{\partial x}$ . (b) In  $z$ -direction where  $\frac{\partial \tau_z}{\partial y} = \frac{\partial p}{\partial z}$ .

FIGURE 2.—Assumed forces acting on fluid element.

the general case, two additional shearing vectors should be shown acting on the sides of the element, but these are considered negligible.

Assuming that static equilibrium of an incompressible fluid prevails and that inertia forces are negligible, the summation of forces in the  $x$ -direction and separately in the  $z$ -direction results in the following relationships between shearing and normal pressures. In the following discussion, because of similar mathematical treatment, equations applying in the  $z$ -direction are developed in parallel with equations in the  $x$ -direction. Thus

$$\frac{\partial \tau_x}{\partial y} = \frac{\partial p}{\partial x} \quad (2)$$

$$\frac{\partial \tau_z}{\partial y} = \frac{\partial p}{\partial z} \quad (2a)$$

The shearing stress acting between layers of viscous fluid in laminar flow is dependent upon the inverse slope of the velocity profile as given below:

$$\tau_x = \mu \frac{\partial u}{\partial y} \quad (3)$$

$$\tau_z = \mu \frac{\partial w}{\partial y} \quad (3a)$$

where  $\mu$  is the absolute viscosity of the fluid.

Differentiating equations (3) and (3a) with respect to  $y$  and substituting in equations (2) and (2a) give

$$\mu \frac{\partial^2 u}{\partial y^2} = \frac{\partial p}{\partial x} \quad (4)$$

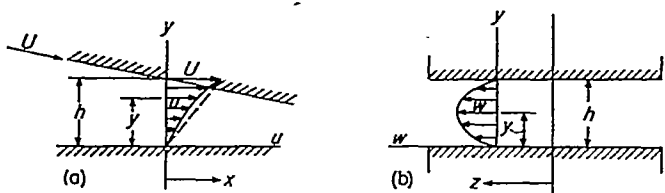
$$\mu \frac{\partial^2 w}{\partial y^2} = \frac{\partial p}{\partial z} \quad (4a)$$

Equations (4) and (4a) are integrated to give variations of velocities  $u$  and  $w$  with respect to  $y$  (velocity profiles) by assuming that the viscosity and pressure are constant throughout the oil film thickness. Thus,  $\mu$ ,  $\partial p/\partial x$ , and  $\partial p/\partial z$  are constants with respect to  $y$ . Assuming that no slip exists between fluid and bearing surfaces, the boundary conditions are:  $u=0$  and  $w=0$  at  $y=0$ ;  $u=U$  and  $w=0$  at  $y=h$ . Integrating equations (4) and (4a) yields

$$u = \frac{Uy}{h} + \frac{1}{2\mu} \frac{\partial p}{\partial x} y(y-h) \quad (5)$$

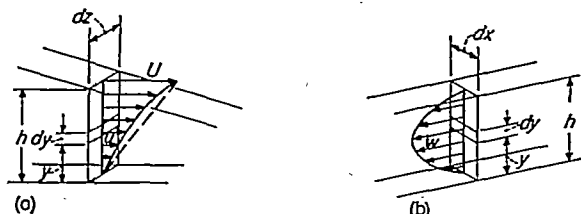
$$w = \frac{1}{2\mu} \frac{\partial p}{\partial z} y(y-h) \quad (5a)$$

The forms of equations (5) and (5a) show that the velocity profiles are parabolic. It may be seen that for the velocity profile in the circumferential direction the first term of equation (5) gives a linear velocity profile indicated by the dashed line in figure 3 and the second term makes the profile parabolic.



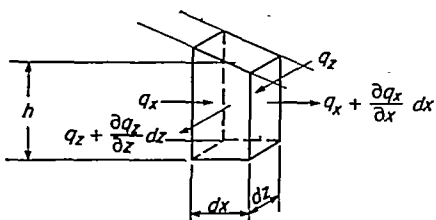
(a) In  $x$ -direction where  $u = \frac{Uy}{h} + \frac{1}{2\mu} \frac{\partial p}{\partial x} y(y-h)$ .  
 (b) In  $z$ -direction where  $w = \frac{1}{2\mu} \frac{\partial p}{\partial z} y(y-h)$ .

FIGURE 3.—Velocity profiles in oil film.



(a) In  $x$ -direction where  $q_x = \left( \frac{Uh}{2} - \frac{h^3}{12\mu} \frac{\partial p}{\partial x} \right) dz$ .  
 (b) In  $z$ -direction where  $q_z = \left( -\frac{h^3}{12\mu} \frac{\partial p}{\partial z} \right) dx$ .

FIGURE 4.—Quantity of flow per unit time through elemental plane.

FIGURE 5.—Quantities of flow entering and leaving fluid element as given by  $\frac{\partial q_x}{\partial x} dx + \frac{\partial q_z}{\partial z} dz = 0$ .

The velocity profiles may be used to determine the quantities of fluid flow per unit of time in the  $x$ - and  $z$ -directions. The quantity  $q_x$  is the flow in the  $x$ -direction through a transverse plane having the area  $h dz$ ; the quantity  $q_z$  is the flow in the  $z$ -direction through an area  $h dx$  as shown in figure 4. These quantities may be expressed as follows:

$$q_x = \int_0^h u dy dz = \left( \frac{Uh}{2} - \frac{h^3}{12\mu} \frac{\partial p}{\partial x} \right) dz \quad (6)$$

$$q_z = \int_0^h w dy dx = \left( -\frac{h^3}{12\mu} \frac{\partial p}{\partial z} \right) dx \quad (6a)$$

Considering the flow of fluid through an elemental volume of dimensions  $h$ ,  $dx$ , and  $dz$  as shown in figure 5, an equation of continuity of flow may be written since it is required that the quantity entering must be equal to the quantity leaving. A steady state of flow is assumed. Thus,

$$q_x + q_z = q_x + \frac{\partial q_x}{\partial x} dx + q_z + \frac{\partial q_z}{\partial z} dz$$

$$\frac{\partial q_x}{\partial x} dx + \frac{\partial q_z}{\partial z} dz = 0 \quad (7)$$

Equation (7) indicates that the increase of the rate of flow in one direction is equal to the decrease in the rate of flow in the other direction. Substituting in equation (7) the proper derivatives of equations (6) and (6a) and assuming that the viscosity is constant in all regions of the fluid result in Reynolds' equation in the form of equation (1).

#### PRINCIPAL ASSUMPTION FOR SHORT BEARINGS

The following analysis results in the pressure-distribution function as given by Michell and Cardullo. The principal simplifying assumption made in this analysis is one regarding equation (6) for the flow in the  $x$ -direction, namely, that, of the two right-hand terms, the second is negligible compared with the first. Referring to figure 3(a), the first term represents the flow as given by the area of the triangular portion of the velocity profile; the area of the profile between the dashed line and the parabolic curve is considered to be small by comparison. This does not mean that  $\partial p / \partial x$  is necessarily small, but that the term  $h^3 / 12\mu (\partial p / \partial x)$  is small. Thus, it is assumed that

$$q_x = \frac{Uh}{2} dz \quad (8)$$

Comparing equation (8) with equation (6), it may be seen that the assumption made results eventually in the omission of the first of the left-hand terms in Reynolds' equation (eq. (1)). The solution which follows will therefore include that part of the circumferential flow proportional to journal surface velocity and varying film thickness but will neglect the effect of circumferential pressure gradient on this flow. Any change in circumferential flow will directly influence the axial flow and the axial pressure gradient.

The shape of the bearing as given by the length  $l$  and the diameter  $d$  affects the relationship between the circumferential and axial pressure gradients. Both gradients depend upon the distance from the point of maximum film pressure to a boundary where the pressure is zero. For the circumferential gradient this distance is related to  $\pi d/4$  and it is related to  $l/2$  for the axial gradient. Thus, as  $l$  becomes small compared with  $d$ , the circumferential gradient becomes small compared with the axial gradient.

Neglecting the effect of circumferential pressure gradient on the flow, the rates of change of flow in the  $z$ - and  $z$ -directions are given by differentiating equations (8) and (6a):

$$\frac{\partial q_x}{\partial x} = \frac{U}{2} \frac{\partial h}{\partial x} dz \quad (9)$$

$$\frac{\partial q_z}{\partial z} = \frac{\partial}{\partial z} \left( -\frac{h^3}{12\mu} \frac{\partial p}{\partial z} \right) dx \quad (9a)$$

Equation (9) is a result of the above assumption and indicates that, when the flow is into the converging oil film, the decrease in flow in the circumferential direction is due primarily to a decrease in film thickness. Substituting equations (9) and (9a) in the continuity equation (7) results in the simple differential equation:

$$\frac{\partial}{\partial z} \left( h^3 \frac{\partial p}{\partial z} \right) = 6\mu U \frac{\partial h}{\partial x} \quad (10)$$

Referring to Reynolds' equation (eq. (1)) it is seen that equation (10) lacks the first left-hand term. Since  $h$  is not a function of  $z$ , equation (10) may be written:

$$\frac{d^2p}{dz^2} = \frac{6\mu U}{h^3} \frac{dh}{dx} \quad (10a)$$

Further, since none of the terms on the right-hand side of equation (10a) are functions of  $z$ , double integration gives

$$p = \frac{6\mu U}{h^3} \frac{dh}{dx} \frac{z^2}{2} + C_1 z + C_2$$

The constant of integration  $C_1$  may be evaluated from the boundary condition that  $dp/dz=0$  at  $z=0$  for symmetrical flow about the transverse plane of symmetry at the center of the bearing. From the condition that pressures at the ends of the bearing are at the atmospheric datum of zero gage pressure,  $C_2$  may be determined from  $p=0$  at  $z=\pm l/2$ . Thus the pressure distribution as a function of  $x$  and  $z$  is given by

$$p = \frac{3\mu U}{h^3} \frac{dh}{dx} \left( z^2 - \frac{l^2}{4} \right) \quad (11)$$

Since  $dx=r d\theta$ , equation (11) may be given in polar coordinates

$$p = \frac{3\mu U}{rh^3} \frac{dh}{d\theta} \left( z^2 - \frac{l^2}{4} \right) \quad (11a)$$

For the journal axis displaced  $e$  with respect to the bearing axis, the film thickness may be approximated by

$$h = c_r + e \cos \theta = c_r (1 + n \cos \theta) \quad (12)$$

where  $c_r$  is the radial clearance and  $n$  is the eccentricity ratio, or attitude of the journal with respect to bearing, given by the ratio  $e/c_r$ . As shown in figure 1,  $\theta$  is measured from the station where the film is of maximum thickness. Thus

$$\frac{dh}{d\theta} = -c_r n \sin \theta \quad (12a)$$

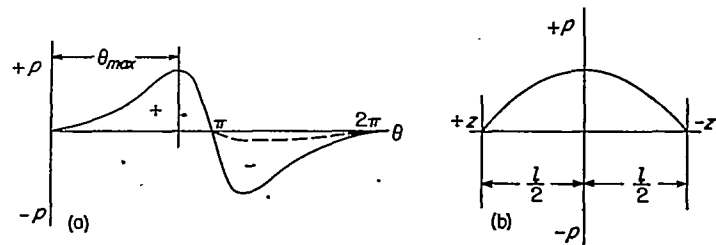
Substituting equations (12) and (12a) in equation (11a)

$$p = \frac{3\mu U}{rc_r^3} \left( \frac{l^2}{4} - z^2 \right) \frac{n \sin \theta}{(1 + n \cos \theta)^3} \quad (13)$$

Expression (13) shows that the pressure distribution is parabolic in the  $z$ -direction and sinusoidal in the circumferential direction giving zero pressures at  $z=\pm l/2$  and  $\theta=m\pi$  where  $m$  is an integer. Figure 6 shows the approximate forms of the distributions in the  $x$ - and  $z$ -directions.

#### EXTENSION OF ANALYSIS RESULTING IN BEARING PERFORMANCE CHARACTERISTICS

As discussed in another section of this report, experimental data show that the pressure-distribution function as given by equation (13) is in good agreement with short-journal-bearing behavior. This apparent agreement has led to the extension of the analysis to include the determination of other bearing characteristics, given below, which the pressure-distribution function makes possible.



(a) In  $x$ -direction. (b) In  $z$ -direction.

FIGURE 6.—Pressure distribution in a full cylindrical bearing as given by  $p = \frac{3\mu U}{rc_r^3} \left( \frac{l^2}{4} - z^2 \right) \frac{n \sin \theta}{(1 + n \cos \theta)^3}$ .

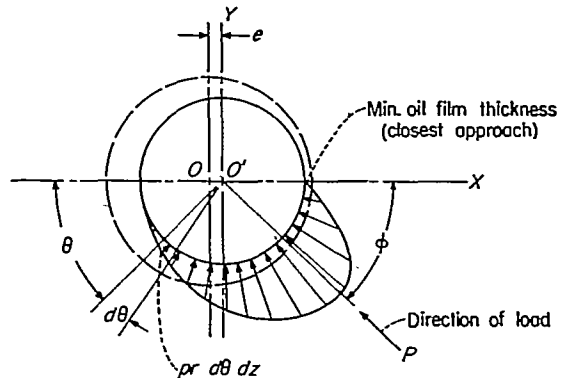


FIGURE 7.—System of coordinates chosen for integration of pressures and determination of attitude angle  $\phi$ .

#### EXTENT OF PRESSURE IN FULL CYLINDRICAL BEARINGS

As shown in figure 6 the circumferential pressure distribution given by equation (13) is positive in the converging film  $0 < \theta < \pi$  and is negative in the diverging film  $\pi < \theta < 2\pi$ . The maximum negative pressure is shown to be equal in magnitude to the maximum positive pressure, a condition which does not appear to exist except in very lightly loaded bearings. A negative pressure of small magnitude not exceeding that of atmospheric pressure, as shown by the dashed line in figure 6, is possible. In the absence of a high datum pressure, the negative pressures are assumed to be of negligible magnitude. It is assumed for moderately and heavily loaded bearings that the positive pressure region from  $\theta=0$  to  $\theta=\pi$ , as given by equation (13), carries the total load.

#### CAPACITY NUMBER $C_a$ AND LOAD NUMBER $1/C_a$

The external load  $P$  may be related to pressures induced in the oil film by performing certain integrations. Choosing  $X$ - and  $Y$ -axes as shown in figure 7, the integrations of pressures on the journal in the directions of these axes will give components  $P_x$  and  $P_y$  of the resultant force which is equal to  $P$ . The integral expressions for  $P_x$  and  $P_y$  are

$$P_x = -2 \int_0^\pi \int_0^{l/2} pr \cos \theta d\theta dz$$

$$P_y = 2 \int_0^\pi \int_0^{l/2} pr \sin \theta d\theta dz$$

Substituting equation (13) for  $p$  and integrating with respect to  $z$ :

$$P_x = -\frac{\mu U l^3}{2c_r^2} \int_0^\pi \frac{n \sin \theta \cos \theta}{(1+n \cos \theta)^3} d\theta \quad (14)$$

$$P_y = \frac{\mu U l^3}{2c_r^2} \int_0^\pi \frac{n \sin^2 \theta}{(1+n \cos \theta)^3} d\theta \quad (14a)$$

Employing Sommerfeld's mathematical technique (see appendix), the integrations with respect to  $\theta$  yield

$$P_x = \frac{\mu U l^3}{c_r^2} \frac{n^2}{(1-n^2)^2} \quad (15)$$

$$P_y = \frac{\mu U l^3}{4c_r^2} \frac{\pi n}{(1-n^2)^{3/2}} \quad (15a)$$

The applied load is given by

$$P = \sqrt{P_x^2 + P_y^2} = \frac{\mu U l^3}{4c_r^2} \frac{n}{(1-n^2)^2} [\pi^2 (1-n^2) + 16n^2]^{1/2} \quad (16)$$

Substituting  $P = p' l d$  and  $U = \pi d N'$  gives

$$\frac{\mu N'}{p'} \left( \frac{d}{c_d} \right)^2 \left( \frac{l}{d} \right)^2 = \frac{(1-n^2)^2}{\pi n} \left[ \frac{1}{\pi^2 (1-n^2) + 16n^2} \right]^{1/2}$$

The left-hand term is a grouping of bearing variables in nondimensional form and is seen to be dependent upon the eccentricity ratio, or attitude,  $n$ . This term is the capacity number  $C_n$  and may be recognized as the Sommerfeld number  $S$  times the square of the length-diameter ratio. Thus,

$$C_n = S \left( \frac{l}{d} \right)^2 = \frac{(1-n^2)^2}{\pi n} \left[ \frac{1}{\pi^2 (1-n^2) + 16n^2} \right]^{1/2} \quad (17)$$

Equation (17) indicates that the curve of eccentricity ratio as a function of the known bearing variables in the capacity number is a single line for different  $l/d$  ratios. Eccentricity ratio may also be shown as a function of the load number  $1/C_n$  giving a curve of  $n$  as a direction function of load.

#### ATTITUDE ANGLE $\phi$

The angular position of the line of action of the load  $P$  with respect to the location of the minimum film thickness, or point of closest approach, is the attitude angle  $\phi$ , as shown in figure 7, which may be determined from:

$$\tan \phi = \frac{P_y}{P_x} = \frac{\pi (1-n^2)^{1/2}}{4 n} \quad (18)$$

Figure 8 shows the journal bearing reoriented such that the load line of action is vertical.

As shown in equation (18), the attitude angle depends directly on eccentricity ratio such that a single polar curve of  $n$  against  $\phi$  applies for different  $l/d$  ratios.

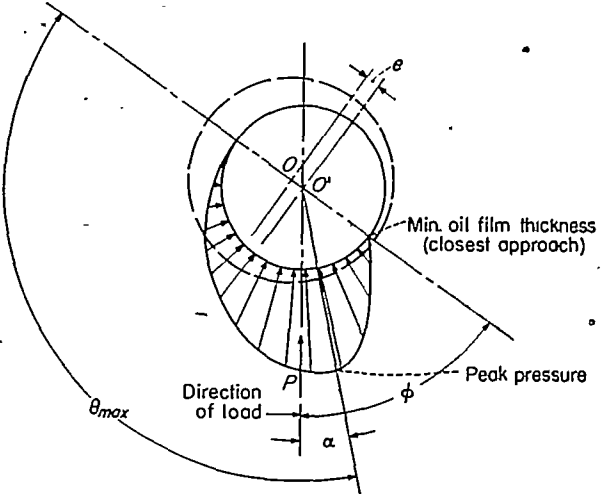


FIGURE 8.—Diagram showing attitude angle  $\phi$ , maximum-pressure angle  $\theta_{max}$ , and peak-pressure angle  $\alpha$ .

#### FRICITION RATIO $F/F_0$ AND FRICTION VARIABLE $f$

Because of the assumed linear velocity profile in the oil film in the circumferential direction, the shearing stress at any location  $\theta$  may be expressed as

$$\tau_x = \mu \frac{\partial u}{\partial y} = \mu \frac{U}{h}$$

The circumferential friction force  $F$  may be evaluated by the following integral:

$$F = \int_0^{2\pi} \tau_x l r d\theta = \int_0^{2\pi} \mu \frac{U}{h} l r d\theta$$

With  $h = c_r (1+n \cos \theta)$ , then

$$F = \frac{\mu U l r}{c_r} \int_0^{2\pi} \frac{d\theta}{(1+n \cos \theta)} = \frac{\mu U l r}{c_r} \frac{2\pi}{(1-n^2)^{1/2}} \quad (19)$$

The coefficient of friction  $f$  is commonly defined as the ratio of friction force to the applied load:

$$f = \frac{F}{P}$$

$$= \frac{\mu U l r}{P c_r} \frac{2\pi}{(1-n^2)^{1/2}}$$

$$f \left( \frac{r}{c_r} \right) \left( \frac{l}{d} \right)^2 = \frac{\mu N'}{p'} \left( \frac{r}{c_r} \right)^2 \left( \frac{l}{d} \right)^2 \frac{2\pi^2}{(1-n^2)^{1/2}}$$

$$f_v = f \left( \frac{d}{c_a} \right) \left( \frac{l}{d} \right)^2$$

$$= C_n \frac{2\pi^2}{(1-n^2)^{1/2}} \quad (20)$$

The first equivalent of  $f_v$  in equation (20) is the friction variable representing a nondimensional grouping of bearing variables including the coefficient of friction. The friction variable is basically dependent upon the eccentricity ratio as indicated by the last equivalent which also includes the capacity number. Since capacity number is a function of  $n$ , friction variable may be plotted against capacity number or load number.

Another nondimensional number including the circumferential friction force  $F$  may be determined from equation (19) as follows:

$$F = \frac{\mu U l r}{c_r} \frac{2\pi}{(1-n^2)^{1/2}} = \mu d l N' \left( \frac{r}{c_r} \right) \frac{2\pi^2}{(1-n^2)^{1/2}}$$

$$\frac{F}{2\pi^2 \mu d l N' \left( \frac{d}{c_a} \right)} = \frac{F}{F_o} = \frac{1}{(1-n^2)^{1/2}} \quad (21)$$

$$F_o = 2\pi^2 \mu d l N' \left( \frac{d}{c_a} \right) \quad (22)$$

Friction force  $F_o$  is the well-known Petroff value of friction force at zero load. The friction ratio  $F/F_o$  as given by equation (21) shows the increase in friction force above the Petroff value as increasing load is applied. A single curve applicable to all  $l/d$  ratios results from plotting friction ratio with capacity number or load number. Plotting  $F/F_o$  with load number shows directly the increase in friction with load. Since friction ratio is nondimensional, it applies to friction torque as well as friction force.

#### OIL FLOW NUMBER $q_n$ AND OIL FLOW FACTOR $q$

Equation (6a) may be used to determine the rate of oil flow discharging from the two ends of the converging wedge. Proper substitution for  $h$  and  $dp/dz$  gives the following expression for the axial flow at any point in the oil film:

$$q_s = \frac{U c_r n z}{2} \sin \theta d\theta$$

At the ends of the bearing:

$$(q_s)_{z=\pm l/2} = \pm \frac{U c_r n l}{4} \sin \theta d\theta$$

The above equations indicate that the axial flow will be outward from the bearing in the region of the converging film  $0 < \theta < \pi$  where the pressures are positive. They also show that in order to develop negative pressures in the film at  $\pi < \theta < 2\pi$  the oil flow must be axially inward. A reservoir of fluid must be available at the ends of the bearing as a

source of supply. The rate of outward axial oil flow at the ends of the bearing from the region of positive pressure is given by the following integral:

$$Q_r = 2 \int_0^\pi \frac{U c_r n l}{4} \sin \theta d\theta$$

$$= U c_r n l$$

$$= \pi d l c_a \frac{N'}{2} n \quad (23)$$

Equation (23) gives the flow which is the result of hydrodynamic action of the load-carrying film in the converging wedge, and it is seen to depend upon the eccentricity ratio  $n$ . Assuming an outward or positive flow from the diverging wedge, the rate of flow to be supplied to the bearing through an inlet hole or grooves on the unloaded side of the bearing must be equal to or greater than that given by  $Q_r$  in equation (23) which may be looked upon as the required rate of flow for the converging film. Equation (23) in the following nondimensional form is the required oil flow number:

$$q_n = \frac{Q_r}{\pi d l c_a \frac{N'}{2} n} = n \quad (24)$$

The required oil flow number is seen to be numerically equal to the eccentricity ratio. The curves of  $q_n$  against  $C_n$  and  $n$  against  $C_n$  are identical.

The total rate of flow  $Q$  includes the positive flow from the unloaded area of the bearing as well as the flow from the converging film and should therefore be greater than  $Q_r$  for proper performance of the bearing. The ratio of total rate of flow to the required rate is termed the oil flow factor  $q$ :

$$q = \frac{Q}{Q_r} = \frac{Q}{\pi d l c_a \frac{N'}{2} n} \quad (25)$$

#### PEAK-PRESSURE RATIO $k$

The peak pressure in the fluid film may be determined from equation (13) at  $z=0$  and  $\theta=\theta_{max}$ , where  $\theta_{max}$  is the angular position of maximum film pressure. Differentiating equation (13) with respect to  $\theta$  and maximizing:

$$\theta_{max} = \arccos \left[ \frac{1}{4n} (1 - \sqrt{1 + 24n^2}) \right] \quad (26)$$

$$p_{max} = \frac{3\mu U l^2}{4 r c_r^2} \left[ \frac{n \sin \theta_{max}}{(1 + n \cos \theta_{max})^3} \right]$$

The ratio of peak pressure to the unit pressure, where unit pressure  $p'$  is defined as the load divided by the projected area of the bearing, is termed peak-pressure ratio  $k$ :

$$k = \frac{p_{max}}{p'} = C_n \frac{6\pi n \sin \theta_{max}}{(1 + n \cos \theta_{max})^3} \quad (27)$$

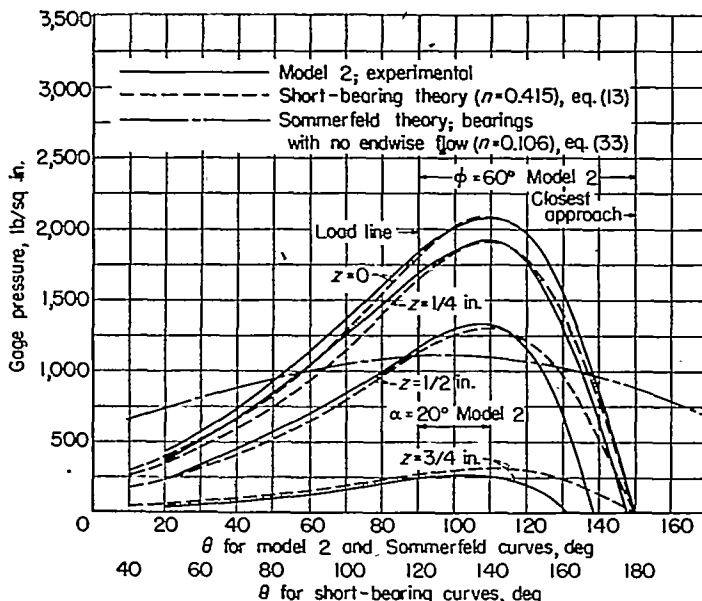


FIGURE 9.—Comparison of theoretical pressure distribution with experimental pressure distribution of model 2 of reference 13. Load, 2,200 pounds; speed, 5,000 rpm; average temperature, 197° F; viscosity,  $2.42 \times 10^{-6}$  reyn; bearing length,  $1\frac{1}{2}$  inches; bearing diameter,  $1\frac{1}{8}$  inches; radial clearance at 197° F, 0.001 inch.

Since  $\theta_{max}$  and  $C_n$  are functions of  $n$ , peak-pressure ratio will plot as a single line against capacity number or load number.

#### PEAK-PRESSURE ANGLE $\alpha$

The angular position of the location of peak pressure with respect to the load line is the peak-pressure angle  $\alpha$  as shown in figure 8. Peak-pressure angle may be determined from the following expression:

$$\alpha = \phi - (180^\circ - \theta_{max}) \quad (28)$$

Equations (18), (26), and (28) show that peak-pressure angle is directly dependent on eccentricity ratio. However, since  $n$  is a function of  $C_n$ ,  $\alpha$  may be plotted with capacity number or load number to give a single line.

Analytical curves as given by the foregoing equations are shown plotted in figures 9 to 19. Although the eccentricity ratio  $n$  is the fundamental variable in all of the equations, it is useful in almost all instances to plot curves using capacity number  $C_n$ , or load number  $1/C_n$ , as the basic variable because it can be obtained from the known variables of load, speed, clearance,  $l/d$  ratio, and viscosity in nondimensional form.

#### COMPARISON OF ANALYTICAL CURVES WITH EXPERIMENTAL DATA

Figure 9 compares the analytical oil film pressure distribution from equation (13) with the pressure distribution experi-

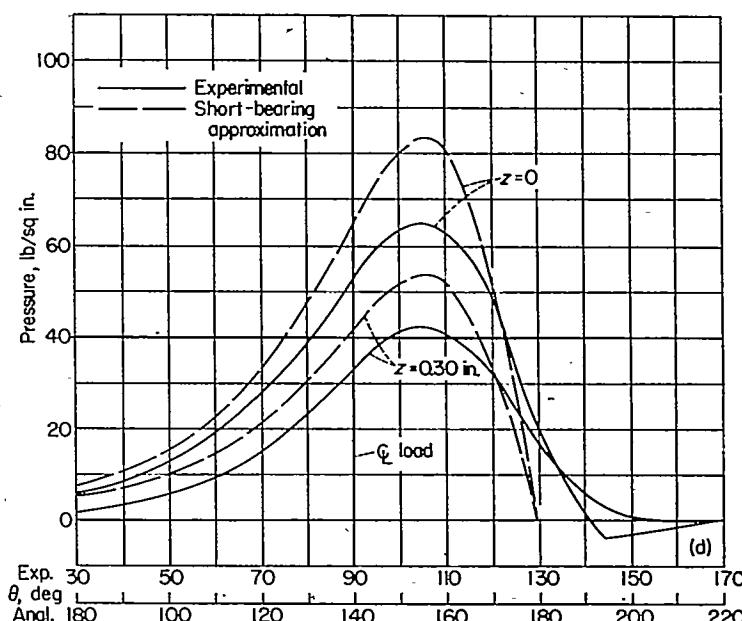
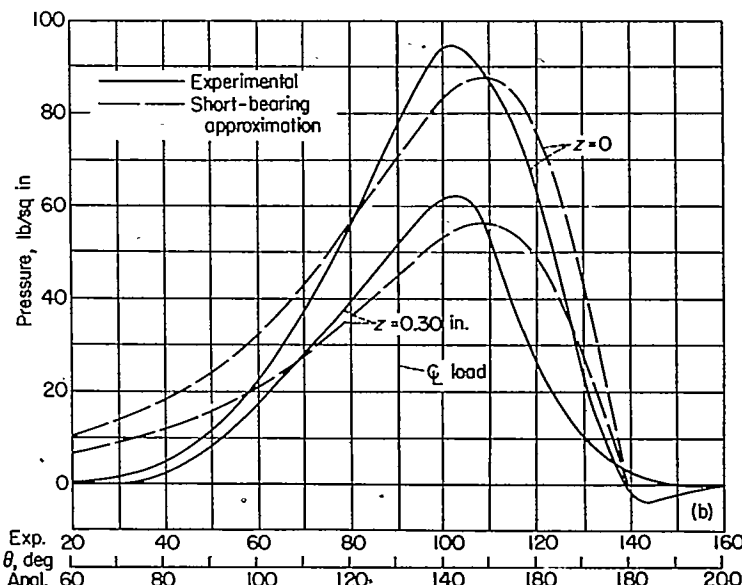
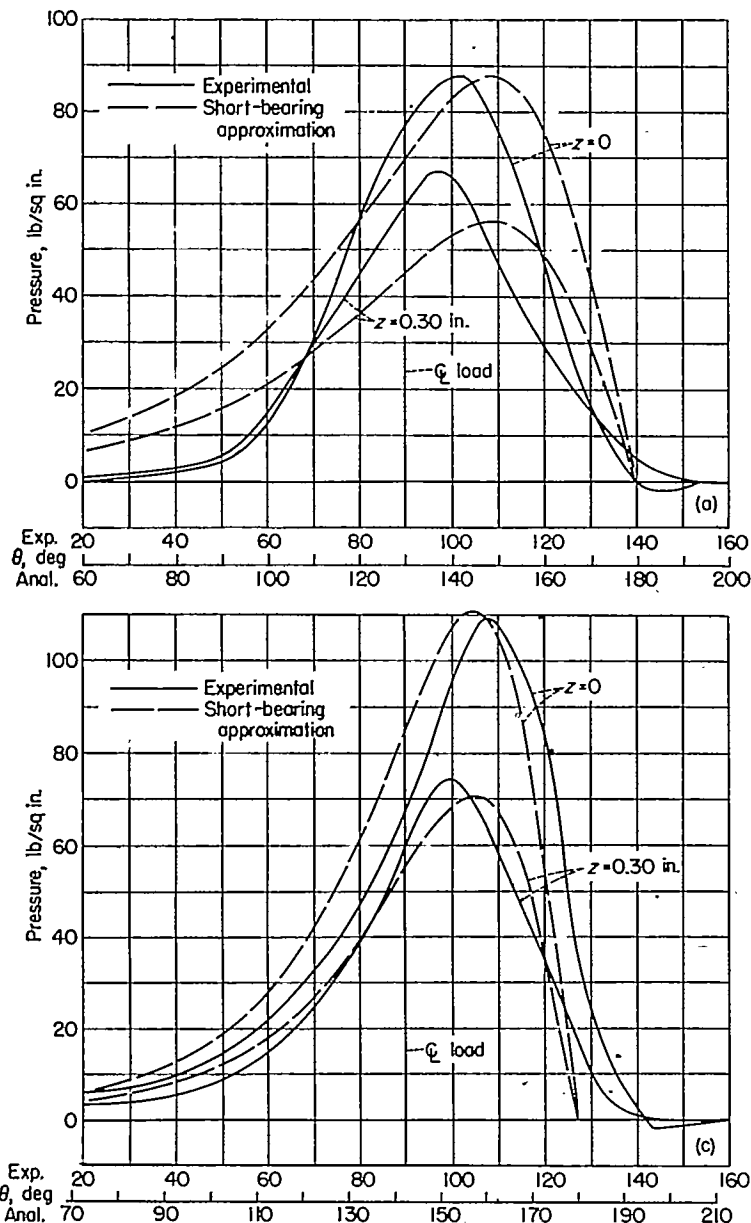
mentally measured by DuBois, Mabie, and Ocvirk (ref. 13). These data were taken on a  $1\frac{1}{2}$ -by  $1\frac{1}{2}$ -inch bearing operating at 5,000 rpm with a load of 2,200 pounds. The close agreement shown for  $l/d=1$  suggested further investigation. The pressure distribution in the oil film given by equation (13) is also shown in figure 10 for comparison with experimental data by McKee and McKee (ref. 11) for a 1-inch-long by  $\frac{1}{2}$ -inch-diameter bearing at speeds up to 592 rpm and a load of 25 pounds.

Curves of peak-pressure ratio from equation (27) and peak-pressure angle from equation (28) are shown as a function of capacity number in figures 11 and 12. The experimental values were obtained from pressure distributions of figures 9 and 10. An interesting feature is that the maximum angular displacement of the peak pressure as given by  $\alpha$  is approximately 20° at  $n \approx 0.4$  and  $C_n=0.15$ . For comparison, if the extent of the oil film is considered to be 360°, as in the Sommerfeld solution, the value of  $\alpha$  reaches a maximum of 90° at  $n=1.0$ .

The relatively close agreement shown by the data on pressure distribution and the rather meager amount of data available on eccentric displacement of the shaft in the journal encouraged the establishment of an experimental program to provide data for comparison with the analytical curves. The greater part of the experimental data in figures 13 to 19 was obtained by this investigation on a  $1\frac{1}{2}$ -inch-diameter bearing with length-diameter ratios of 1,  $\frac{1}{2}$ , and  $\frac{1}{4}$ , speeds of 500 to 6,000 rpm, and unit bearing pressure on projected area up to 900 pounds per square inch. Description of the experimental apparatus and tests is given later in this report. Certain experimental data on oil flow by McKee (ref. 14) are also shown in figure 19.

Attitude angle as determined from equation (18) is shown as a function of eccentricity ratio by the polar curve in figure 13; experimental data obtained by this investigation are given for comparison. The attitude angle gives the angular position of the line through the bearing and journal centers with respect to the line of action of the applied load. At values of  $n$  near zero the line of centers is nearly normal to the load line and becomes parallel to the load line at  $n=1.0$ . Experimental data for short bearings as obtained by this investigation are shown in figure 13 for comparison with the analytical curve. The manner in which these data were obtained is given in another section of this report. Bradford and Davenport (ref. 15) have obtained an experimental curve whose shape is similar to the curve of figure 13. As may be seen, the path of the journal is slightly within a semicircle.

Eccentricity-ratio curves from equation (17) are presented in figures 14 and 15 with capacity number as abscissa in one curve and load number, in the other. The same experimental data are shown in both figures 14 and 15.



(a) Test 1;  $P=25$  pounds,  $N=565$  rpm,  $\mu=42.9$  centipoises, and  $n=0.555$ .

(b) Test 2;  $P=25$  pounds,  $N=592$  rpm,  $\mu=39.4$  centipoises, and  $n=0.561$ .

(c) Test 3;  $P=25$  pounds,  $N=244$  rpm,  $\mu=36.5$  centipoises, and  $n=0.712$ .

(d) Test 4;  $P=20$  pounds,  $N=244$  rpm,  $\mu=34.4$  centipoises, and  $n=0.688$ .

FIGURE 10.—Comparison of analytical pressure distributions with experimental pressure distributions from tests by McKee and McKee (ref. 11).  $l=1.0$  inch,  $d=0.8703$  inch, and  $c_r=0.0025$  inch

Friction characteristics of short bearings are given by the curves in figures 16 and 17. Equation (20) gives the values for the analytical curve of friction variable against the capacity number in figure 16, and equation (21) determines the curve of friction ratio against load number in figure 17. From the experimental data shown, it may be seen that effect of load on friction is more clearly shown by

friction ratio (fig. 17) than by friction variable (fig. 16).

Oil flow number as a function of capacity number from equation (24) is represented by the analytical curve of figure 18. The experimental values of oil flow number shown in figure 18 are obviously not in agreement with the analytical values since the analytical values represent only the rate of flow from the converging wedge and the experimental values

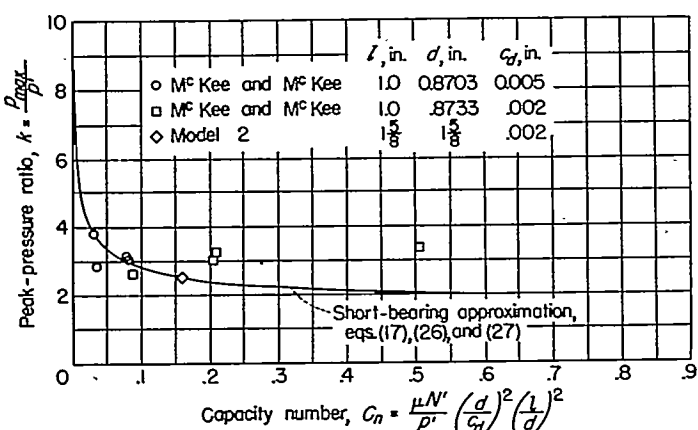


FIGURE 11.—Plot of peak-pressure ratio against capacity number for comparison of experimental data with analytical curve for short bearings. Data by McKee and McKee taken from reference 11 and data for model 2, from reference 13.

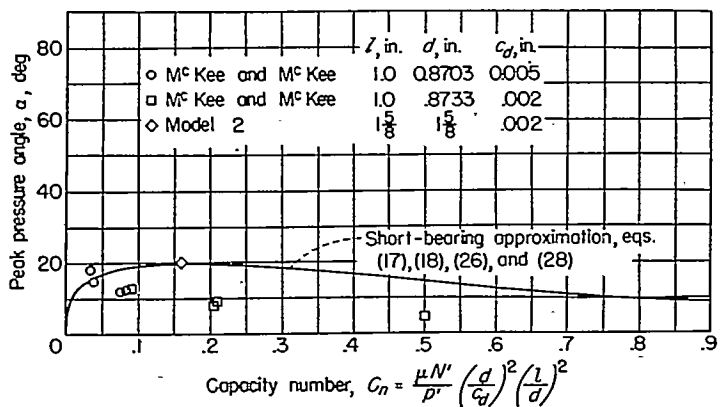


FIGURE 12.—Plot of peak-pressure angle against capacity number for comparison of experimental data with analytical curve for short bearings. Data by McKee and McKee taken from reference 11 and data for model 2, from reference 13.

represent the total flow. An inspection of the experimental data in figure 18 indicates that the flow rate in excess of that from the converging film is dependent upon inlet oil pressure, speed, and  $l/d$  ratio. Speculating that oil film viscosity and clearance also affect the excess flow rate, all the variables affecting total flow rate are grouped nondimensionally in a form similar to the capacity number but using the inlet oil pressure  $p_o$  in place of the unit bearing load  $p'$ , giving a variable termed inlet-pressure capacity number  $C_{p_o}$  as follows:

$$C_{p_o} = \frac{\mu N'}{p_o} \left( \frac{d}{c_d} \right)^2 \left( \frac{l}{d} \right)^2 = C_n \frac{p'}{p_o} \quad (29)$$

A curve of oil flow factor  $q$ , the ratio of total flow rate to the flow rate from the converging wedge (eq. (25)), as a function of the inlet-pressure capacity number is shown in figure 19. As shown, the widely scattered experimental data of figure 18 result in a single curve when plotted according to the nondimensional ordinates of figure 19. The experimental data by McKee (ref. 14) for bearings with a single oil feed hole show excellent agreement with the experimental

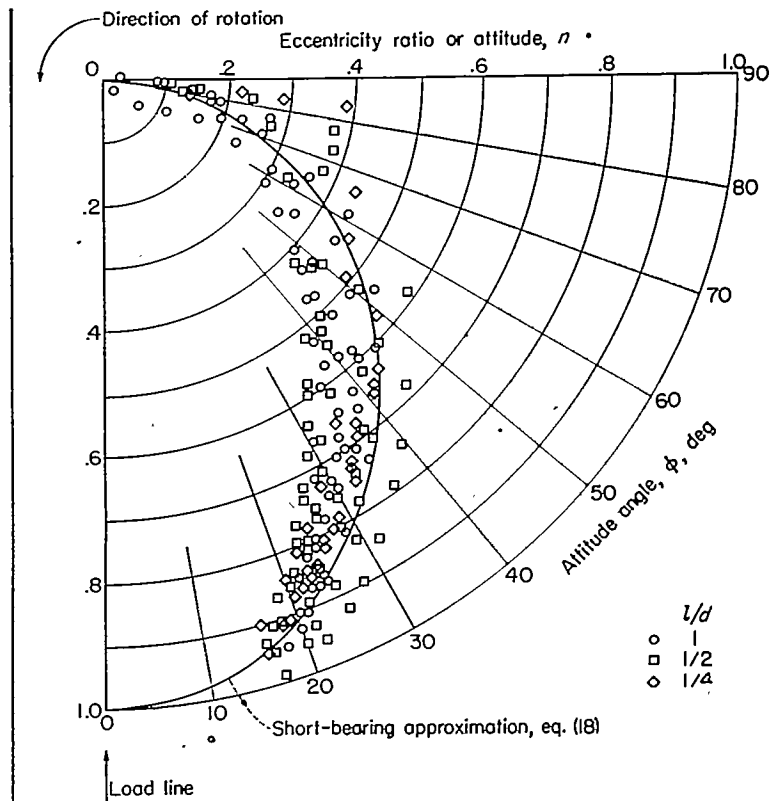


FIGURE 13.—Plot of eccentricity ratio against attitude angle for comparison of experimental data for  $l/d$  of 1,  $1/2$ , and  $1/4$  with analytical curve for short bearings. Experimental data: Bearing diameter, 1 $\frac{1}{2}$  inches; bearing, bronze; journal, steel; diametral clearance, 0.00232 and 0.00264 inch; inlet pressure of SAE 10 oil  $p_o$  fed through one  $\frac{1}{16}$ -inch-diameter hole, 40 and 100 pounds per square inch; speed, 500 to 6,000 rpm; load, 0 to 1,450 pounds; bearing pressure, 0 to 760 pounds per square inch; average bearing temperature  $\frac{1}{16}$  inch from oil film  $T_{as}$ ,  $114^\circ$  to  $160^\circ$  F.

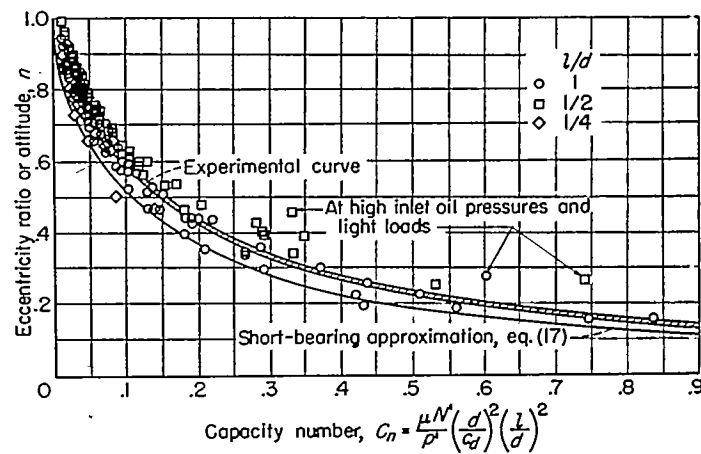


FIGURE 14.—Plot of eccentricity ratio against capacity number for comparison of experimental data for  $l/d$  of 1,  $1/2$ , and  $1/4$  with analytical curve for short bearings. Experimental data: Bearing diameter, 1 $\frac{1}{2}$  inches; bearing, bronze; journal, steel; diametral clearance, 0.00232 and 0.00264 inch; inlet pressure of SAE 10 oil  $p_o$  fed through one  $\frac{1}{16}$ -inch-diameter hole, 40 and 100 pounds per square inch; speed, 500 to 6,000 rpm; load, 0 to 1,450 pounds; bearing pressure, 0 to 760 pounds per square inch; average bearing temperature  $\frac{1}{16}$  inch from oil film  $T_{as}$ ,  $114^\circ$  to  $160^\circ$  F.

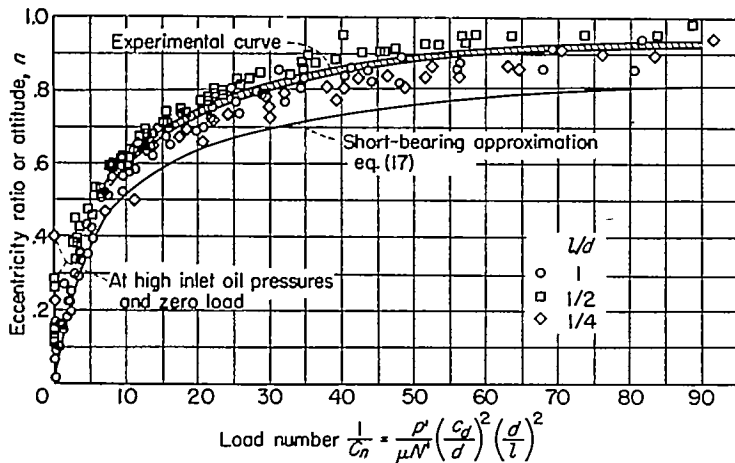


FIGURE 15.—Plot of eccentricity ratio against load number for comparison of experimental data for  $l/d$  of 1,  $\frac{1}{2}$ , and  $\frac{1}{4}$  with analytical curve for short bearings. Experimental data: Bearing diameter,  $1\frac{1}{2}$  inches; bearing, bronze; journal, steel; diametral clearance, 0.00232 and 0.00264 inch; inlet pressure of SAE 10 oil  $p_o$  fed through one  $\frac{1}{8}$ -inch-diameter hole, 40 and 100 pounds per square inch; speed, 500 to 6,000 rpm; load, 0 to 1,450 pounds; bearing pressure, 0 to 760 pounds per square inch; average bearing temperature  $\frac{1}{16}$  inch from oil film  $T_{av}$ ,  $115^\circ$  to  $160^\circ$  F.

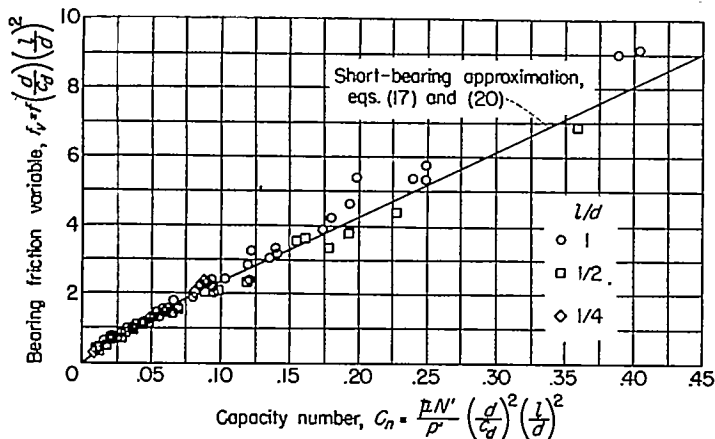


FIGURE 16.—Plot of bearing friction variable against capacity number for comparison of experimental data for  $l/d$  of 1,  $\frac{1}{2}$ , and  $\frac{1}{4}$  with analytical curve for short bearings. Experimental data: Bearing diameter,  $1\frac{1}{2}$  inches; bearing, bronze; journal, steel; diametral clearance, 0.00232 and 0.00264 inch; inlet pressure of SAE 10 oil  $p_o$  fed through one  $\frac{1}{8}$ -inch-diameter hole, 40 and 100 pounds per square inch; speed, 500 to 6,000 rpm; load, 0 to 1,750 pounds; bearing pressure, 0 to 900 pounds per square inch; average bearing temperature  $\frac{1}{16}$  inch from oil film  $T_{av}$ ,  $115^\circ$  to  $161^\circ$  F.

data of this investigation. The McKee data for an axial oil inlet groove form a parallel line at an increased rate of oil flow. The McKee data were obtained at the National Bureau of Standards using a bearing 2.06 inches in diameter with SAE 20 oil at speeds of 2,030 and 3,040 rpm, loads of 1,553 and 3,008 pounds, and temperatures from  $203^\circ$  to  $228^\circ$  F.

#### DESCRIPTION OF APPARATUS

A photograph of the bearing testing machine used in the experiments appears in figure 20. The manner in which the test elements were supported and loaded is shown in

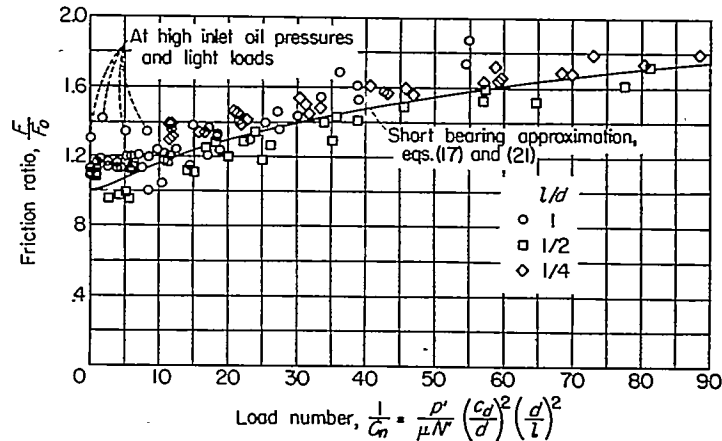


FIGURE 17.—Plot of friction ratio against load number for comparison of experimental data for  $l/d$  of 1,  $\frac{1}{2}$ , and  $\frac{1}{4}$  with analytical curve for short bearings. Experimental data: Bearing diameter,  $1\frac{1}{2}$  inches; bearing, bronze; journal, steel; diametral clearance, 0.00232 and 0.00264 inch; inlet pressure of SAE 10 oil  $p_o$  fed through one  $\frac{1}{8}$ -inch-diameter hole, 40 and 100 pounds per square inch; speed, 500 to 6,000 rpm; load, 0 to 1,750 pounds; bearing pressure, 0 to 900 pounds per square inch; average bearing temperature  $\frac{1}{16}$  inch from oil film  $T_{av}$ ,  $115^\circ$  to  $161^\circ$  F.

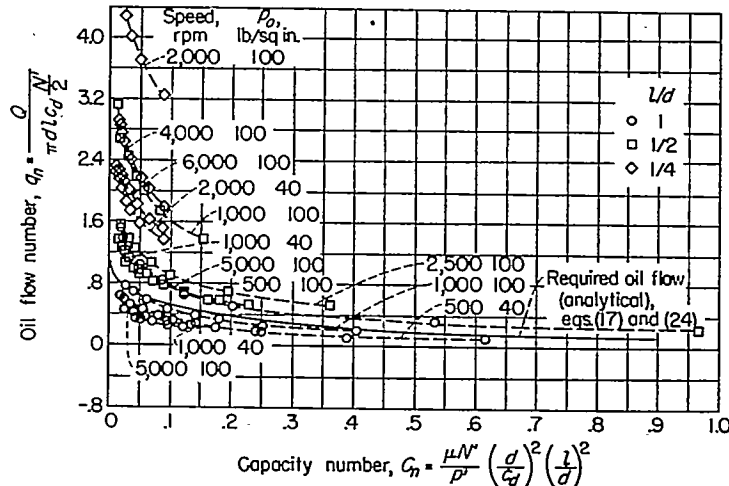


FIGURE 18.—Curves of oil flow number against capacity number for comparison of experimental total oil flow with theoretically required flow through loaded portion of oil film for  $l/d$  of 1,  $\frac{1}{2}$ , and  $\frac{1}{4}$ . Experimental data: Bearing diameter,  $1\frac{1}{2}$  inches; bearing, bronze; journal, steel; diametral clearance, 0.00232 and 0.00264 inch; inlet pressure of SAE 10 oil  $p_o$  fed through one  $\frac{1}{8}$ -inch-diameter hole, 40 and 100 pounds per square inch; speed, 500 to 6,000 rpm; load, 0 to 1,750 pounds; bearing pressure, 0 to 900 pounds per square inch; average bearing temperature  $\frac{1}{16}$  inch from oil film  $T_{av}$ ,  $115^\circ$  to  $161^\circ$  F.

figures 21, 22, and 23. In addition, figure 23 illustrates diagrammatically the torquemeter used for friction-torque measurements and the means for collecting the oil flowing through the test bearing. Figures 24 and 25 show the mechanical system which measured the displacements of the journal at the ends of the bearing. The locations of thermocouples measuring bearing temperatures are given in figure 26.

A bronze bearing and two steel shafts of  $1\frac{1}{8}$ -inch nominal diameter were used as shown in figures 21 and 22 giving a single bearing for length-diameter ratios of 2 and 1, and a

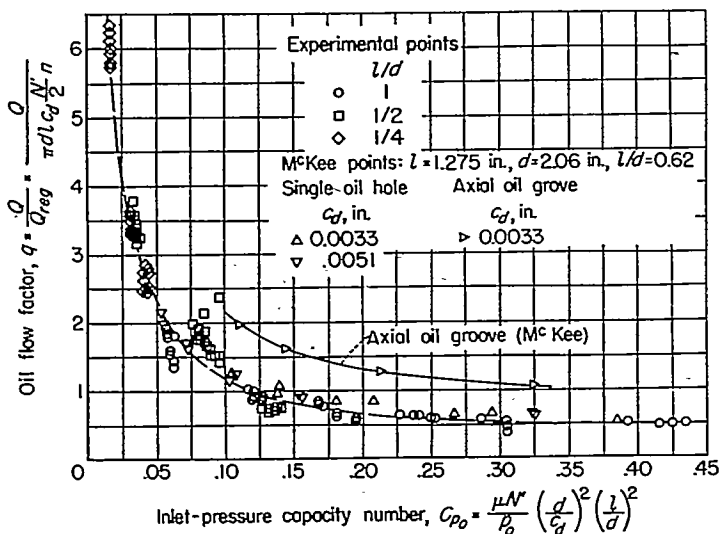


FIGURE 19.—Curve of oil flow factor against inlet-pressure capacity number. Experimental data are given for  $l/d$  of 1,  $\frac{1}{2}$ , and  $\frac{1}{4}$ . Oil flow factor is ratio of experimental total flow to flow required through loaded portion of oil film by short-bearing approximation. Experimental data: Bearing diameter,  $1\frac{1}{8}$  inches; bearing, bronze; journal, steel; diametral clearance, 0.00232 and 0.00264 inch; inlet pressure of SAE 10 oil  $p_0$ , fed through one  $\frac{1}{8}$ -inch-diameter hole opposite load line, 40 and 100 pounds per square inch; speed, 500 to 6,000 rpm; load, 0 to 1,750 pounds; bearing pressure, 0 to 900 pounds per square inch; average bearing temperature  $\frac{1}{16}$  inch from oil film  $T_{av}$ , 115° to 161° F. Experimental oil flow,  $Q = q \left( \pi d l c_d \frac{N' n}{2} \right)$ . McKee data are taken from reference 14.

double bearing with a drained area between for the narrower bearings having length-diameter ratios of  $1/2$  and  $1/4$ . In every case, each bearing was lubricated by a single  $\frac{1}{8}$ -inch oil hole in the center as shown.

A special boring bar, of the type developed by the Battelle Memorial Institute, was constructed to bore the bearing to an accuracy of 50 millionths of an inch (0.000050 in.) as indicated by a special Federal hole gage, and the shafts were ground and lapped to the same accuracy as shown by a Pratt & Whitney supermicrometer.

Clearance was determined by measurement of the static displacement or rattle of the clean shaft in the bearing under reversing load. As shown in figures 21 and 22 the average clearances determined were 0.00264 inch for the single journal and 0.00232 inch for the double journal at room temperature.

#### MEASUREMENT OF JOURNAL DISPLACEMENT

The coordinate displacements of the journal with respect to the bearing during running were measured by the mechanical arrangement shown in figures 24 and 25. Horizontal and vertical motions of the shaft at stations beyond the ends of the bearing were transmitted by the bronze riders on levers or bell cranks through vertical rods to four

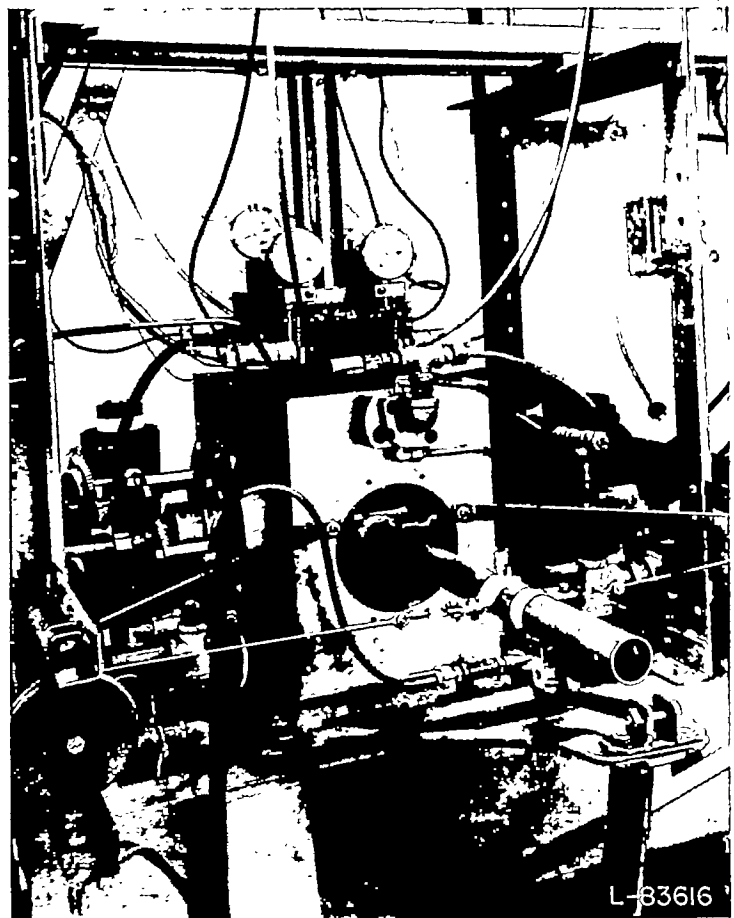


FIGURE 20.—Bearing testing machine used in experiments. Equipment includes variable-speed electric drive to 10,000 rpm, direct hydraulic loading mechanism, misaligning loading mechanism, and heater, filter, and pressure pump for lubricating oil. Measurements made include journal displacement, friction torque, oil flow, bearing temperatures, and, with accessories, oil film pressures.

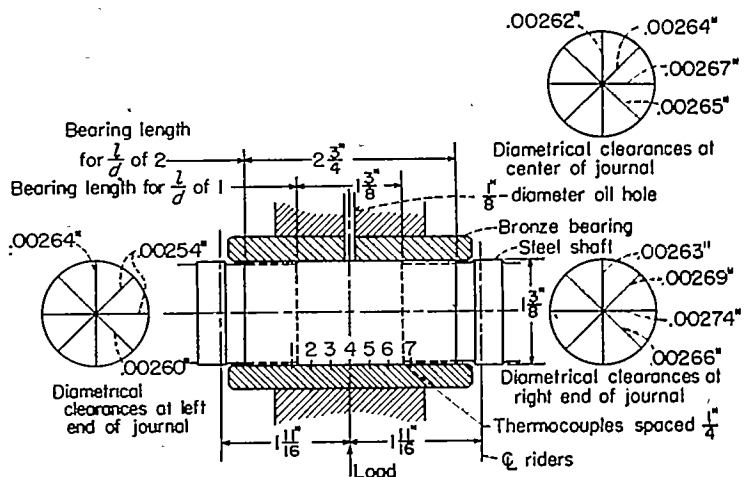


FIGURE 21.—Test shaft with single journal as used in experiments at  $l/d$  of 2 and 1. Average diametral clearance, 0.00264 inch.

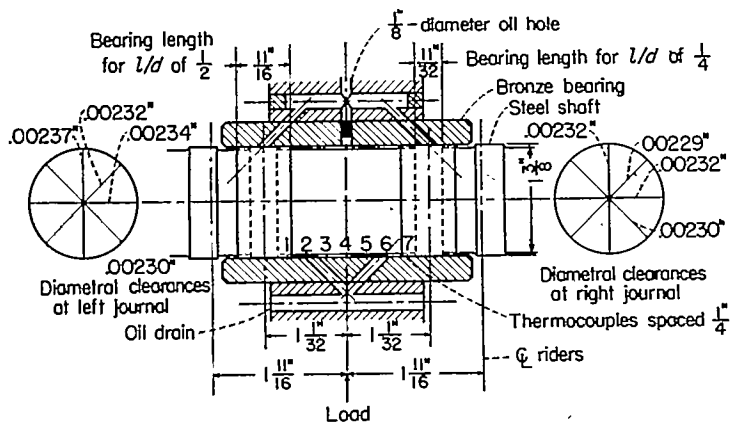


FIGURE 22.—Test shaft with two journals as used in experiments at  $l/d$  of  $\frac{1}{2}$  and  $\frac{1}{4}$ . Average diametral clearance, 0.00232 inch.

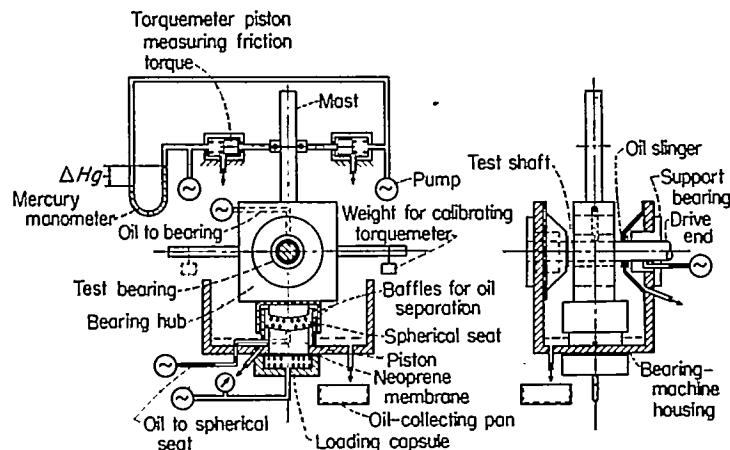


FIGURE 23.—Schematic diagram of apparatus for measuring friction torque on test bearing and oil flow through test bearing.

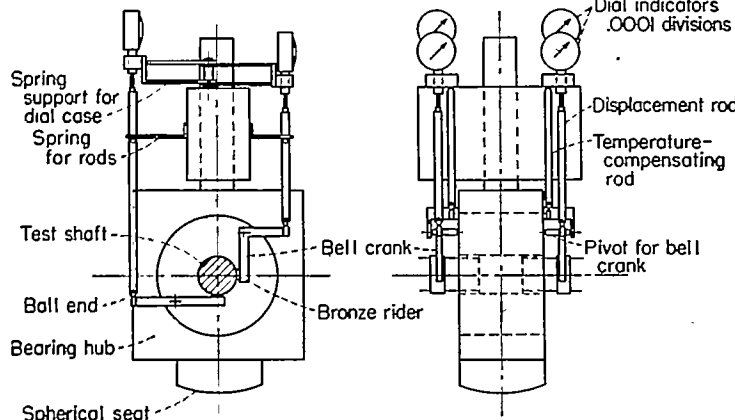


FIGURE 24.—Mechanical system for measuring displacement of journal with respect to bearing.

dial indicators having 0.0001-inch divisions. The rods were held against the ball ends of the bell cranks by flat springs attached to the mast on the bearing hub. In order to eliminate large dial readings due to thermal expansion of

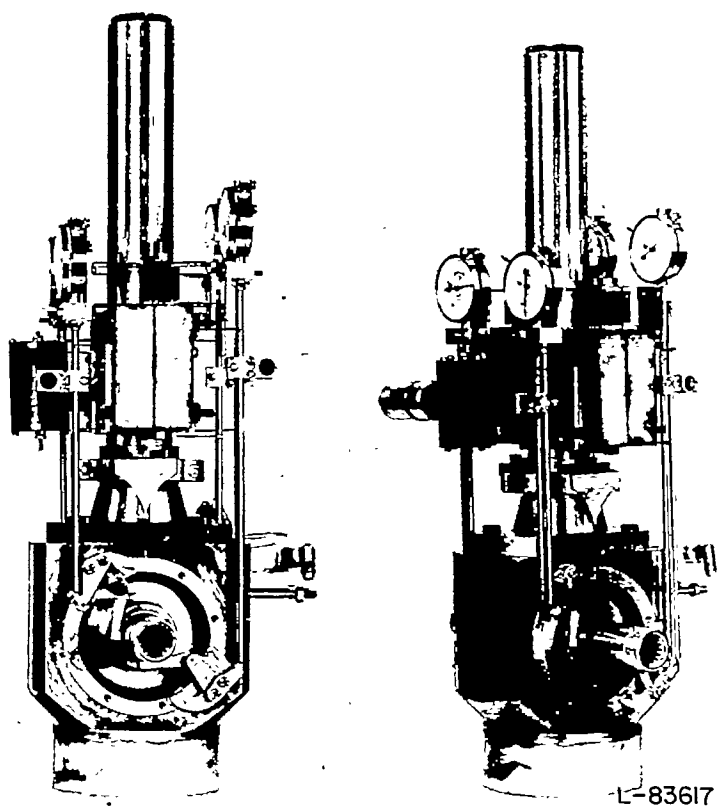


FIGURE 25.—Mechanical and photoelectric apparatus for measuring journal displacements with respect to bearing. Journal displacements are transmitted by levers and rods to dial indicators, which are used for steady-state conditions, and to photoelectric cells, for dynamic conditions.

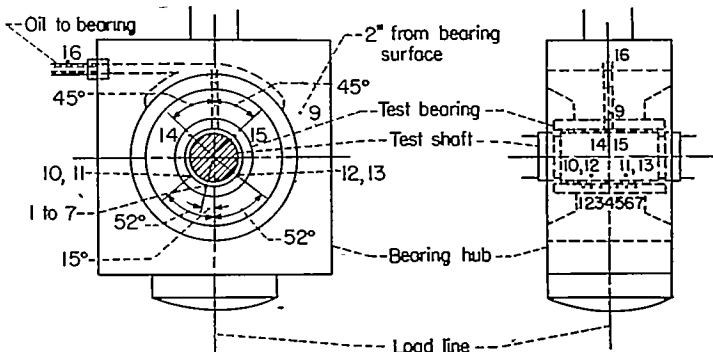


FIGURE 26.—Diagram of thermocouple locations. Bearing thermocouples are located  $\frac{1}{8}$  inch from bearing surface.

the rods, a second set of similar parallel rods, intended for temperature compensation, moved the dial cases approximately the same amount the dial stems were moved by thermal expansion.

As shown in figures 20 and 25, a second system was available for the measurement of displacement. This system, developed by Phelan (ref. 16), is a photoelectric method particularly suited to indicate dynamic displacements on oscilloscopes. However, it was found to be more rapid and

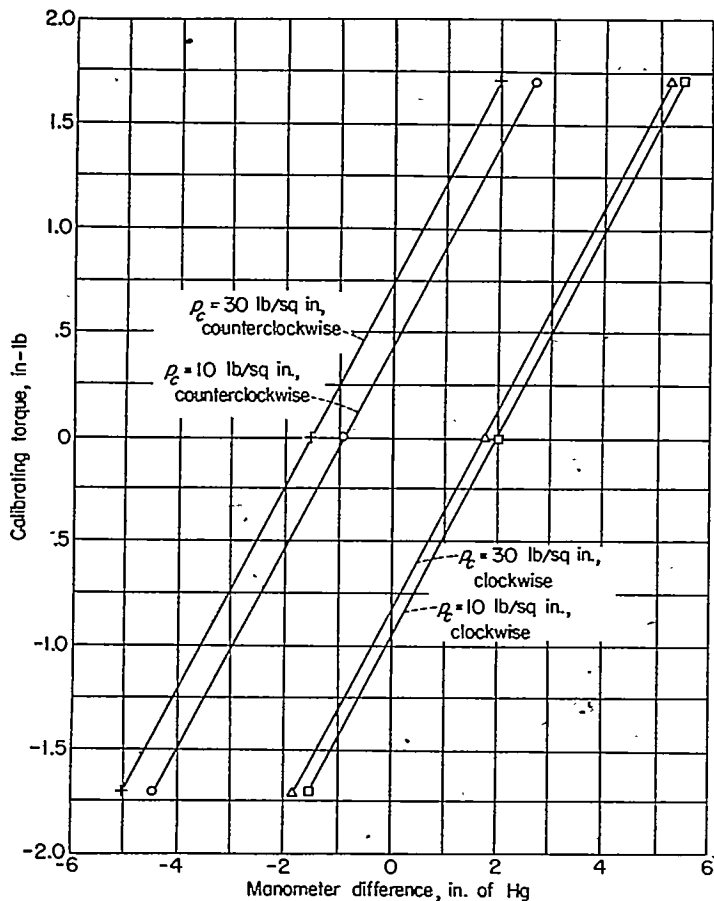


FIGURE 27.—Typical calibration curves for torquemeter used to measure friction torque on test bearing. Average slope of curves is calibration factor  $F_c$  giving friction torque per inch of difference in levels of mercury columns of manometer,  $F_c = 0.485 \frac{\text{in-lb}}{\text{in. of Hg}}$ . See table II for data.

convenient to take direct readings on the dial-indicating system under stable conditions. All of the data for this report were taken from the dial system.

#### MEASUREMENT OF FRICTION AND OIL FLOW

The friction torque on the test bearing was indicated by a hydraulic torquemeter as shown in figure 23. This consisted of two opposed pistons supplied with a flow of oil which drained through ports partially covered by the pistons. A mercury manometer indicated the difference in pressure on the opposed pistons which were floated in their bores by balanced pressure areas. A direct calibration relating applied moment to manometer reading is shown in figure 27. The torquemeter restrained the motion of the test bearing to  $\frac{1}{2}^\circ$  or less under operating conditions.

An SAE 10 oil was used in the experiments on length-diameter ratios of  $1/2$ ,  $1/4$ , and  $1$ , the measured viscosity being shown in figure 28. The oil flow of the test bearing was kept

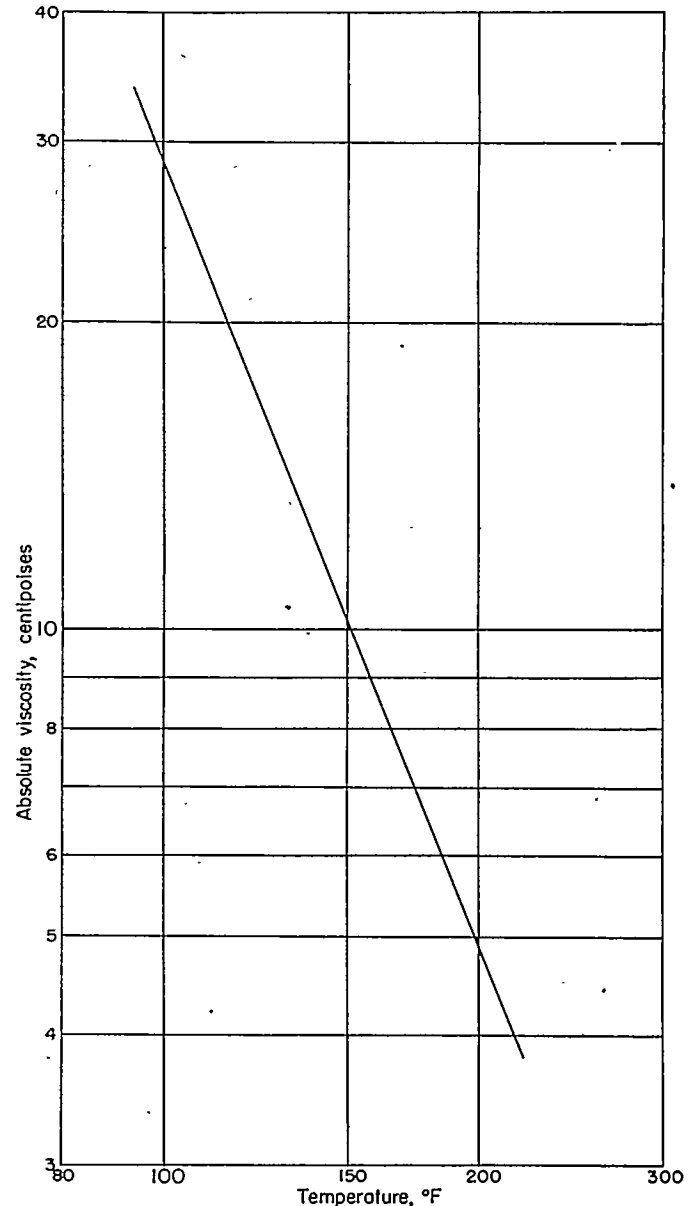


FIGURE 28.—Absolute-viscosity and temperature characteristics of SAE 10 oil used in tests for  $l/d$  of  $1$ ,  $\frac{1}{2}$ , and  $\frac{1}{4}$ . Measurements of viscosity were made in a standard Saybolt viscosimeter.

separate from the oil flow of the support bearings by baffles and slingers and was collected for weighing in a calibrated scale graduated in hundredths of a pound. Bearing temperatures were measured by 14 thermocouples placed in the bearing as shown in figure 26. Iron-constantan thermocouples inserted in 0.094-inch holes to within  $\frac{1}{16}$  inch of the bearing surface were connected to a Leeds & Northrup potentiometer with automatic cold junction compensation and a Fahrenheit scale. A thermocouple attached to the bulb of a glass laboratory thermometer reading ambient temperature checked each set of readings within  $1^\circ$  F.

#### LOADING AND DRIVING SYSTEM

As shown in figure 23 the test bearing was loaded by a pressure capsule containing a piston having an area of 15.02 square inches. The piston head was flush with and sealed by a  $\frac{1}{2}$ -inch-thick Neoprene membrane which permitted a steady pressure to be held by an accumulator. Calibrated pressure gages of varying ranges connected to the capsule gave the load on the bearing. The load from the piston was transmitted to the test-bearing hub through an oil-pressurized spherical seat as shown in figure 23. A flow of light oil forced into relieved quadrant areas in the spherical seat prevented metallic contact in order that the load could be transmitted without resistance to motion of the bearing about its geometric axes. This enabled measurement of friction torque on the bearing and located the line of action of the load at the bearing center. The shaft was directly driven by a 200-ampere aircraft generator acting as a motor, and by field control of this and a similar unit in a motor-generator set a speed range of 500 to 10,000 rpm was attainable.

The apparatus and test procedure are described in greater detail in reference 17.

#### TEST PROCEDURE

For each length-diameter ratio of 1,  $\frac{1}{2}$ , and  $\frac{1}{4}$  two series of experiments were conducted. In the first series, displacements of the journal were measured by the dial-indicator equipment shown in figure 24. Friction torque and oil flow rate were measured in a second series of tests separate from displacement tests because it was necessary to disconnect the dial indicators to eliminate any friction torque due to the riders. Also, oil flow tests could not be made during the displacement tests because the small oil flow used to lubricate the riders mixed with the oil flowing from the test bearing. A brief initial series of tests with  $l/d=2$  is not included as they were completed before the following technique was developed.

#### METHOD OF LOCATING ZERO-LOAD POINT

In the displacement tests, the coordinate locations of each end of the shaft were measured as changes of location from the zero-load position. In order to establish a reading of the dial indicators with the shaft in the center of the bearing clearance at zero load alternate up and down loads were applied with the shaft stationary, and the average of three sets of readings was recorded. The individual readings located points in an arc slightly on each side of a vertical diameter. After a similar procedure in the horizontal plane the machine was started and warmed up, and a capsule pressure of about 4 pounds per square inch was applied to balance the tare weight of the bearing hub and various attachments. With the shaft running and the inlet oil

pressure reduced to 2 to 4 pounds per square inch, the average of the dial readings representing the location of the center of the journal was checked and held within close limits to the center of the bearing as obtained above with the shaft stationary.

The net load applied to the bearing is that due to the difference of the pressure on the loading piston, called capsule pressure, and the pressure of 3.5 to 4.5 pounds per square inch required to balance the weight of the bearing-hub assembly. The displacement is the difference in dial readings from a test load to zero load. This method has the advantage that change in load is plotted against change in displacement.

It was discovered that when running at zero load the bearing required nearly zero oil flow; the dials showed that the journal maintained its position steadily when the inlet oil pressure was reduced to 2 pounds per square inch and the oil flow was a few drops per minute. Increasing the inlet oil pressure caused the journal to displace as though a load had been applied. This effect was more marked as the inlet pressure was further increased and the oil flow increased to a continuous stream.

#### SHAFT-DISPLACEMENT EXPERIMENTS

In making shaft-displacement tests, the zero-load position of the shaft was determined as described, and a warmup period of 20 to 30 minutes was made at constant speed. Variations in displacement were obtained by varying the load at constant speed and constant inlet oil pressure. It was found that by holding a constant speed the variations in temperature were less than  $5^{\circ}\text{F}$  during an increasing-load run.

Displacement data as read from the four dials were then recorded as the load was increased in 10 to 15 increments and then decreased in the same increments to permit averaging of data. A sample log sheet is shown in table I. The same procedure was followed in the opposite direction of rotation so that the data could be averaged for the two rotations. After a varying-load test, the location of the datum point at zero load was rechecked in two directions of rotation to permit averaging out any small change during the test. Wear of the lever rubbing surfaces or riders was usually imperceptible during individual tests but would have been canceled by this method.

For each length-diameter ratio there were experimental runs in each direction of rotation at combinations of constant speed and constant inlet oil pressure. The speeds were 500, 1,000, 2,000, 2,500, 4,000, 5,000, and 6,000 rpm, and the inlet oil pressures were 40 and 100 pounds per square inch. The maximum load on projected area was 760 pounds per square inch, and the maximum oil film temperature was  $160^{\circ}\text{F}$ .

## CONTROL OF WHIRL

At journal speeds of 500 and 1,000 rpm there was little difficulty with vibration even at zero load. However, at zero load at the higher speeds from 2,000 to 5,000 rpm a vibration, or whirl, in a rotating misalignment mode would build up, preventing the reading of displacements. The vibration could be stopped by the application of load, but it was necessary to prevent vibration at zero load in order to use the routine procedure to obtain the position of zero eccentricity. By snubbing the top of the mast and the arm extending laterally from the bearing hub with foam rubber, the vibrations were successfully eliminated, using small snubbing forces parallel to the axis of the shaft. By temporarily removing the snubbers at loads where no vibration would occur, it was found that the snubbers had no effect on the dial-indicator readings.

## FRICTION AND OIL FLOW EXPERIMENTS

Friction torque and oil flow rate were measured simultaneously, with the displacement-measuring apparatus temporarily disconnected in order to eliminate the friction of the riders and the oil flow to them. Changes in friction and oil flow were made by varying the applied load and maintaining the journal speed and inlet oil pressure constant. Before beginning a test, a period of running of approximately 20 to 30 minutes at constant speed was allowed to reach thermal equilibrium. About 10 to 15 increments of increasing load were then applied. At each load, after the oil flow stabilized, the flow rate was determined by collecting the oil in a pan for periods of 1 to 4 minutes and recording the net weight of oil. A sample log sheet is shown in table II. The same procedure was followed for the opposite direction of rotation so that data could be averaged for the two rotations.

Several runs at combinations of constant speed and constant inlet oil pressure were made in each rotational direction for each length-diameter ratio. The speeds were 500, 1,000, 2,000, 2,500, 4,000, 5,000, and 6,000 rpm, and the inlet oil pressures were 40 and 100 pounds per square inch. The maximum load on projected area was 900 pounds per square inch, and the maximum oil film temperature was 161° F.

The foam-rubber snubbers used to eliminate vibration in the displacement experiment were removed because they offered restraint to rotation of the bearing about its axis and interfered with the functioning of the torquemeter. At speeds above 1,000 rpm vibrations were stopped by the application of a small load. Since the condition of zero load is not of great importance in friction and oil flow measurements, data were taken only at loads where no vibration occurred.

## PRECISION

In every run of the friction experiments, calibrations of the torquemeter were made as a check on operating accuracy by applying known weights to the arms extending from the front and rear of the bearing hub as shown in figure 23. Manometer differences corresponding with the known moments, first to the front and then to the rear, are given

in the sample log sheet of table II and are shown plotted in figure 27. More extensive tests with several weights had proven that the result was a straight line. From the many calibrations made, a mean value of the calibration factor  $F_c$  was 0.485 inch-pound of torque per inch of manometer difference. The greatest deviation from the mean was 0.010 or 2 percent.

For reliable functioning of the torquemeter it was necessary to bleed air from the oil lines leading to the manometer at the beginning of each run. Because the torquemeter pistons were hydraulically centered in their bores by three pressure areas, the torquemeter was sensitive enough to measure aerodynamic forces on the bearing hub, and it was necessary to rid the test room of air gusts.

All pressure gages of both the laboratory and commercial grades were calibrated in a dead-weight tester with a capacity of 500 pounds per square inch. Pressure readings were corrected according to calibration curves where necessary. The pressure in the loading capsule was indicated by two pressure gages with different scale ranges. It was found that the pressure gages did not accurately read the capsule pressure due to the tare weight of the test bearing hub unless they were placed at the same level as the loading capsule. By suspending two calibrated 50-pound weights from the lateral arms of the bearing hub, the corresponding increase in capsule pressure showed that the calculation of loading in the low range was of satisfactory accuracy.

The four dial indicators used to measure journal displacements were of laboratory test grade and were graduated in 0.0001-inch divisions. A direct calibration of the indicators was made and in the maximum range during tests of about 13 divisions they were accurate to within one-half division. As the load was increased and then decreased there was often a discrepancy of as much as one-half division in displacement for the same load. By averaging the displacement data for increasing and decreasing loads, the influence of the lag on accuracy of measurement is minimized.

Two aircraft-type tachometers were used, one a centrifugal type having a scale range of 1,000 to 10,000 rpm and the other a 3-second counting type with a range of 0 to 1,750 rpm. The centrifugal tachometer was checked under running conditions by timing the revolution counter of the tachometer. By connecting both tachometers to the test shaft simultaneously at speeds of 1,000 to 1,500 rpm the two tachometers were checked against each other. A portable shop-type tachometer was used to check the lower-range tachometer at 500 rpm.

The direct-reading Fahrenheit scale of the Leeds & Northrup potentiometer having automatic cold-junction compensation was used to measure bearing temperatures from thermocouples and can be read to an accuracy of 1° to 2° F. A thermocouple attached to the bulb of a laboratory-grade thermometer giving ambient temperature near the machine checked the thermometer temperature within 1° F. No direct calibration of the potentiometer was made.

The weighing scale used to measure oil flow was equipped with a scale of 2-pound capacity graduated in hundredths

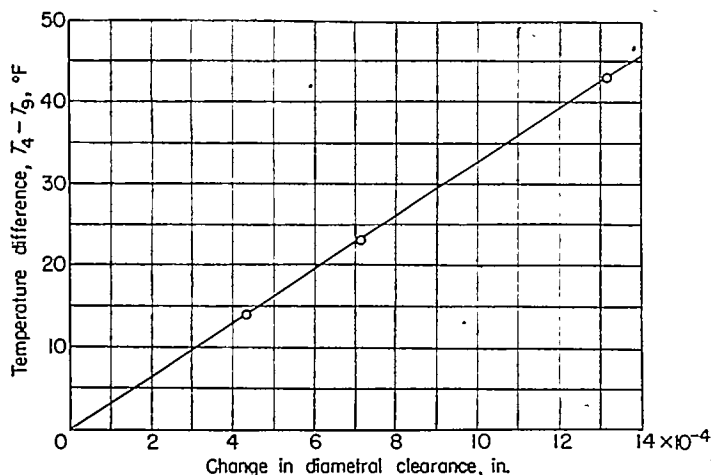


FIGURE 29.—Changes in diametral clearance as function of temperature difference of two points in test-bearing wall.  $T_4$  and  $T_9$  are bearing temperatures at  $\frac{1}{8}$  inch and 2 inches, respectively, from bearing surface. Running clearances of test bearing are determined by subtracting change in clearance from room-temperature clearance.

of a pound which could be read to one-quarter of a division. Chemical balance weights were used to calibrate the scale.

Two Saybolt viscosimeters having two viscosimeter tubes each were available for determining the viscosity of the test oils at various temperatures. The variations in running time from two tubes at a given temperature did not differ more than 1 second.

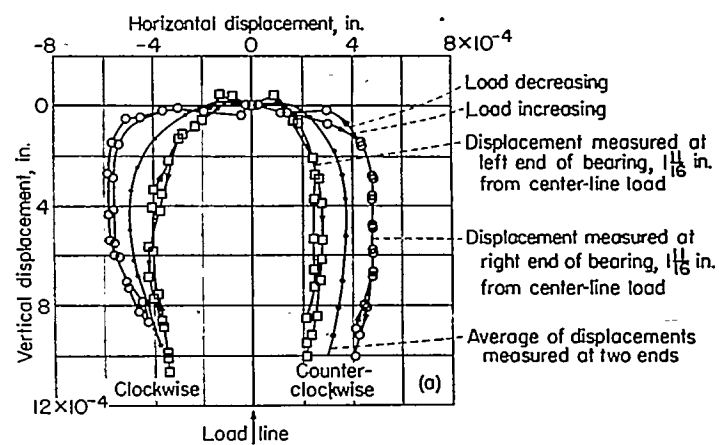
#### REDUCTION OF EXPERIMENTAL DATA

Calculations of several nondimensional quantities are shown in the sample calculation sheets (tables III and IV). The data for the calculations are given in the sample log sheets (tables I and II).

#### CAPACITY NUMBER

The capacity number was calculated from equation (17). The net load applied by the loading piston or capsule was determined as the product of the net capsule pressure in pounds per square inch and the piston area of 15.02 square inches. The weight of the bearing and its attachments required a tare capsule pressure of 4.5 pounds per square inch in the displacement experiments and 3.5 pounds per square inch in the friction and oil flow experiments, which was deducted from the observed pressure.

Bearing clearance was determined by subtracting the change in clearance given by figure 29 from the clearance at room temperature. For the single journals (fig. 21), thermocouples 1 to 7 are in the loaded portion of the bearing. There was little variation between the temperature readings at these locations for a given load. Thermocouple 4 was taken as representative, and the difference of the averages of thermocouples 4 and 9 was determined for the complete run at a given speed. Using this average in figure 29 gives the change in clearance from that at room temperature. For the double journals (fig. 22) where only the end thermocouples are in the loaded region, an average of thermocouples



(a) Displacements of journal measured by riders beyond bearing ends.

FIGURE 30.—Journal displacements with respect to bearing for shaft with two journals of  $l/d$  of  $\frac{1}{4}$ . Steps shown illustrate typical method of determining average eccentricity ratios and attitude angles from displacement data measured beyond ends of bearing. See tables I and III for experimental data and calculations.

1, 4, and 7 was compared with the average of thermocouple 9 to determine the bearing clearance.

Viscosity in the oil film was determined at each load from the average bearing temperature for the two directions of rotation and for increasing and decreasing load. In tests using the single journal, temperature data at thermocouple 4 were taken as representative of the oil film temperature. For the double journals, the average of thermocouples 1 and 7 was more nearly representative because of the location of these points in the narrow loaded area. These temperatures were used to determine viscosity in figure 28.

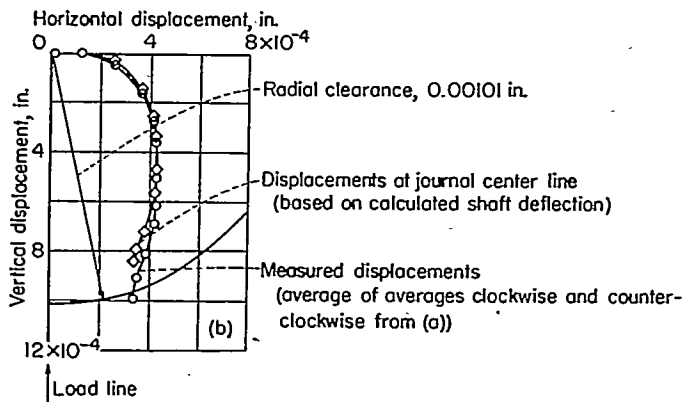
#### ECCENTRICITY RATIO OR ATTITUDE

The eccentricity ratio  $n$  is the ratio of the displacement of the journal axis to the radial clearance given by  $n = e/c_r$ .

Coordinate vertical and horizontal displacements of the shaft were measured at the riders, which are located beyond the ends of the bearing  $1\frac{1}{16}$  inches to the left and to the right of the center line of the load, as shown in figures 21, 22, and 24. To determine the displacement of the test journal, calculations were made of the effect of shaft deflection on the vertical displacements measured at the riders.

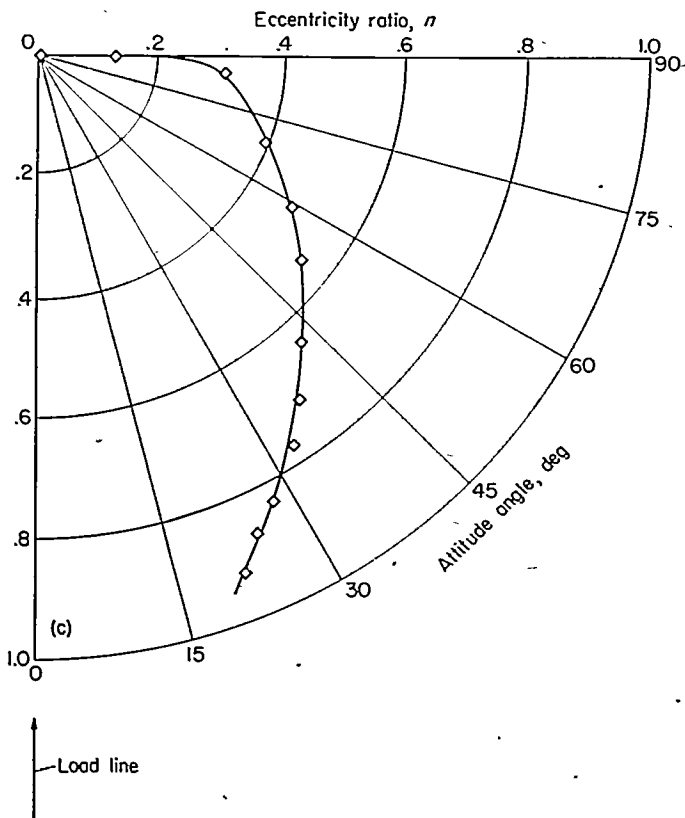
As shown in the sample log sheet of table I, displacement data were taken as the load was increased and then decreased. These data are shown in the sample calculation sheet of table III, then reduced to values of journal displacement from the condition of zero load and a low inlet oil pressure at which, as previously described, it was assumed that the journal and bearing axes were coincident. A plot of these data for the two directions of rotation appears in figure 30(a). The bearing and journal are not ideally accurate cylinders, and there is a departure from symmetry of the displacements at the two ends.

Averages of displacements of the two ends are shown in figure 30(b). The displacements illustrated are typical for the case of a shaft with two journals. In order to determine the displacements of the centers of each journal, calculated values of shaft deflection were subtracted from the measured



(b) Average journal displacements by riders and displacements at journal center line.

FIGURE 30.—Continued:



(c) Displacements at journal center line reduced to eccentricity ratios.

FIGURE 30.—Concluded.

vertical displacements at the riders. The vertical and horizontal components of eccentricity ratio  $n_v$  and  $n_h$  were calculated by dividing the corrected journal displacements by the radial clearance. The plotting of  $n_v$  against  $n_h$  is shown on the polar diagram of figure 30(c) in terms of eccentricity ratio  $n$  and attitude angle  $\phi$ .

In the case of single journals, the method of calculation of eccentricity ratio was similar. Because of the greater length of the single journals and the greater loads applied, shaft bending over the length of the journal was of considerable magnitude at high loads. Since the journal was

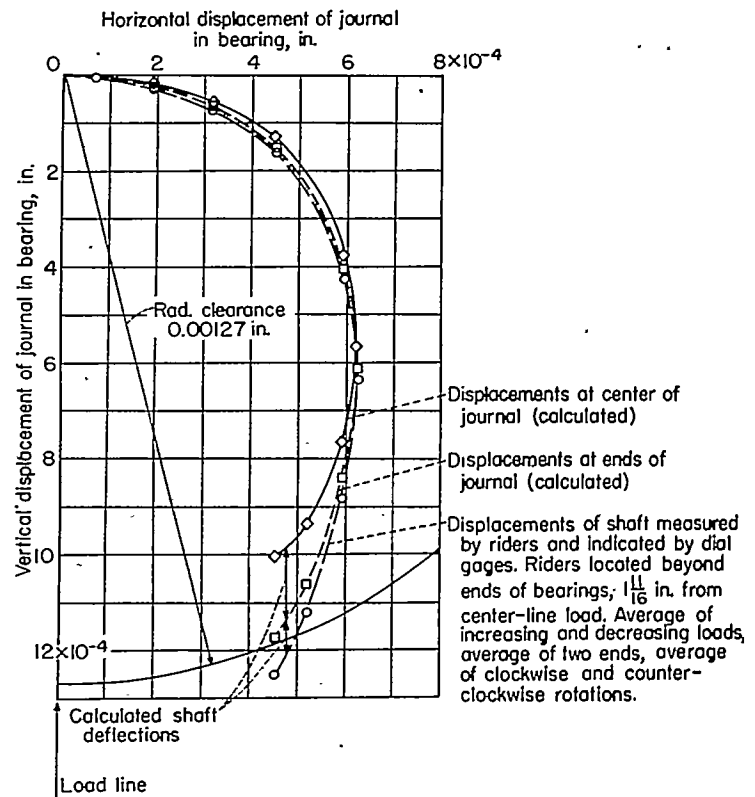


FIGURE 31.—Journal displacements with respect to bearing for shaft with single journal of  $l/d$  of 2. Displacements at ends and center of a bent journal are shown in comparison with displacements measured beyond ends of bearing. Average eccentricity ratios and attitude angles as determined from displacements are shown in figure 32.

bent longitudinally in the shape of a fourth-degree parabola, the displacement and eccentricity ratio at the center of the journal were less than at its ends, as indicated in figures 31 and 32. To simulate the performance of a straight journal, the average eccentricity ratio of a parabolic elastic curve was calculated as representative of the eccentricity ratio of a straight journal (see fig. 32). Four-fifths of the height of the deflection curve within the journal was subtracted from the displacement at the ends.

Eccentricity ratios as a function of capacity number and load number are shown in figures 14 and 15; as a function of attitude angle, they are shown in figure 13.

#### BEARING FRICTION

Experimenters usually distinguish between friction measured on the journal and that measured on the bearing, since the friction torque measured on the bearing is evidently somewhat reduced by the couple resulting from the product of the load and the horizontal component of the displacement. The measured data in this report are the friction measured on the bearing and have been referred to as bearing-friction variables.

Data on friction and shaft displacement were both available so that it was possible to compute the journal friction by adding the couple to the bearing friction. Referring to the column labeled friction variable  $f$ , in table IV, the bearing friction and calculated journal friction for  $l/d=1$  are given as follows:

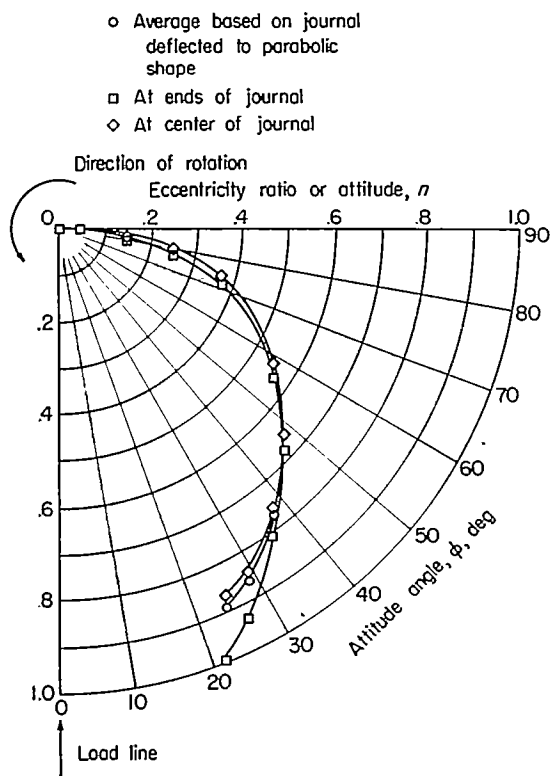


FIGURE 32.—Eccentricity ratios and attitude angles for shaft with single journal of  $l/d$  of 2 as determined from displacements shown in figure 31. The curve of average eccentricity ratios is shown in comparison with eccentricity ratios at ends and center of a bent journal. Experimental data: Speed, 500 rpm; inlet pressure  $p_o$ , 40 pounds per square inch; diametral clearance at room temperature, 0.00264 inch; diametral clearance at bearing temperature  $T_a$ , of  $119^{\circ}$  F, 0.00254 inch; load, 0 to 855 pounds; bearing pressure, 0 to 245 pounds per square inch; AN-09-1010 jet engine oil fed through one  $\frac{1}{8}$ -inch-diameter hole.

Load, $P$ , lb	Bearing friction, $f_b$ ( $\frac{d}{c_d}$ )	Couple, $f_c$ ( $\frac{d}{c_d}$ )	Journal friction, $f_j$ ( $\frac{d}{c_d}$ )	Ratio, $f_b/f_j$
0	0	0	0	1.002
22.5	24.10	.10	24.20	
60.1	9.13	.19	9.32	1.020
97.6	5.70	.27	5.97	1.048
135.1	4.23	.31	4.54	1.073
172.6	3.36	.33	3.69	1.099
210.0	2.36	.34	2.70	1.143
348.0	1.65	.38	1.91	1.230
623.0	1.06	.36	1.41	1.330
848.0	.83	.32	1.15	1.385

In the table above the couple is to be added to the bearing-friction variable and is numerically equal to the horizontal displacement  $n_h$  as follows:

$$f_c \left( \frac{d}{c_d} \right) = \frac{P e \sin \phi}{P r} \left( \frac{r}{c_r} \right) = \frac{e}{c_r} \sin \phi = n \sin \phi = n_h \quad (30)$$

The values of  $n_h$  are those for the run at 1,000 rpm and 40-pound-per-square-inch inlet oil pressure.

Manometer differences indicating bearing friction in inches of mercury for each load condition are shown in the sample log sheet of table II; they are of opposite sign for opposite directions of rotation. For a given load, the absolute values of the manometer differences for the two directions of

rotation were averaged as indicated in the sample calculation sheet of table IV. Multiplication by the calibration factor  $F_c$  gave the friction torque  $M_f$  in inch-pounds. The friction coefficient  $f$  for calculation of the friction variable was determined from  $f = M_f / P r$ . Friction force  $F$  used in the calculation of friction ratio was determined from  $F = M_f / r$ .

The sample calibration-factor curves corresponding with the experimental data of the sample log sheet (table II) are shown in figure 27. Experimental values of bearing-friction variable are shown plotted as a function of capacity number in figure 16. Friction ratios as a function of load number are shown in figure 17.

#### OIL FLOW

As shown in the sample calculation sheet (table IV), oil flow data for the two directions of rotation were averaged at each condition of load. Dividing the weight of oil by the time interval during which it was collected gave the rate of flow  $Q'$  in pounds per minute. Since  $Q$  in the oil flow number must be given in cubic inches per second, a conversion was made from the following expression:

$$Q = Q' \times \frac{1,728}{62.4 \times \text{sp gr}} \times \frac{1}{60} \quad (31)$$

in which sp gr is the measured specific gravity of the oil at oil film temperature. Where double journals were concerned, half of the oil flow was used in calculations of oil flow numbers.

A more complete description of the apparatus, method of test, and reduction of data is given in reference 17.

#### EXPERIMENTAL MEASUREMENT OF FILM PRESSURE DISTRIBUTION

The experimentally measured oil film pressure distribution shown in figure 9 was obtained from reference 13 which included photographs of several plaster models representing measured film pressures in a full journal bearing with babbitt lining. Model 2 of the group of five models represents the pressure distribution for a bearing of  $l/d=1$  acted upon by a normal central load. Model 2 alone is of interest since the other models represent film pressures measured under conditions of misalignment.

As shown in figure 9, the analytical pressure distribution as given by the short-bearing approximation is in very close agreement with the data of model 2. The analytical solution by Sommerfeld is actually not directly comparable because the short-bearing solution is based on an assumed  $180^{\circ}$  of film whereas the Sommerfeld solution assumes a continuous film of  $360^{\circ}$ . Moreover, even if a ruptured film of  $180^{\circ}$  were assumed, the Sommerfeld solution cannot agree with experimental data because the solution gives no variation in film pressure in the axial direction.

The film pressure data of model 2 were taken under the following conditions:  $d=1\frac{1}{8}$  inches,  $l=1\frac{1}{8}$  inches,  $P=2,200$  pounds,  $p'=833$  pounds per square inch,  $N=5,000$  rpm,  $N'=83.3$  rps,  $\mu$  (at  $197^{\circ}$  F) =  $2.42 \times 10^{-6}$  reyn,  $c_d$  (at room temperature) = 0.0033 inch, and  $c_a$  (at  $197^{\circ}$  F) = 0.0020 inch.

Pressure taps in the bearing were located at the center

of the bearing and at  $\frac{1}{4}$ ,  $\frac{1}{2}$ , and  $\frac{3}{4}$  inch each side of the center in a test machine arranged to measure the circumferential pressure distribution shown by the solid lines of figure 9. The model 2 curves represent averages of pressures for the two directions of rotation of the journal and averages at corresponding points each side of the central transverse plane of the bearing.

For this test aviation 1120 oil was preheated to  $140^{\circ}$  F and entered the bearing at the center on the unloaded side through two  $\frac{1}{8}$ -inch-diameter holes  $45^{\circ}$  apart at a pressure of 40 pounds per square inch. The viscosity of the oil is based on the bearing temperature given by a thermocouple located  $\frac{1}{16}$  inch from the bearing surface at the center of the loaded side.

The bearing clearance at operating film temperature is determined from a curve of clearance change against temperature change similar to the curve of figure 29.

The capacity number for model 2 from the above data is 0.159 and the corresponding value of eccentricity ratio from the analytical short-bearing curve of figure 14 is  $n=0.415$ . The analytical short-bearing curves of figure 9 are given by equation (13) for  $n=0.415$  and  $z=0$ ,  $\pm\frac{1}{4}$ ,  $\pm\frac{1}{2}$ , and  $\pm\frac{3}{4}$  inch. Since the angular scale  $\theta$  is different from the scale used in this experiment, two angular scales are required differing by  $90^{\circ}-\phi$ .

Analytical values of peak-pressure ratio, peak-pressure angle, and attitude angle for model 2 are given by the short-bearing curves of figures 11, 12, and 13 for  $C_s=0.159$  and  $n=0.415$ . These values are compared with the experimental values below.

Quantity	Experimental	Analytical
Peak-pressure ratio, $k$ .....	2.49	2.50
Peak-pressure angle, $\alpha$ , deg.....	20	19 $\frac{1}{2}$
Attitude angle, $\phi$ , deg.....	60	60

\* Analytical value of  $\phi$  is measured from load line to location of zero pressure which theoretically coincides with location of minimum film thickness.

The analytical curve in figure 9 given by the Sommerfeld solution is based on the following equations for eccentricity ratio and pressure distribution:

$$S = \frac{\mu N'}{p'} \left( \frac{d}{c_d} \right)^2 = \frac{(2+n^2)(1-n^2)^{1/2}}{12\pi^2 n} \quad (32)$$

$$p = \frac{\mu Ur}{c_r^2} \left[ \frac{6n(2+n \cos \theta) \sin \theta}{(2+n^2)(1+n \cos \theta)^2} \right] + p_s \quad (33)$$

For model 2, equation (32) gives  $n=0.106$ , an eccentricity ratio about one-fourth of that given by the short-bearing

approximation which is a consequence primarily of assuming that the unloaded side of the bearing contributes to the support of the applied load.

In equation (33),  $p_s$  is the film pressure at  $\theta=0$  and  $\pi$ . The value of  $p_s$  may be determined from equation (33) by taking the pressure at  $\theta=(3/2)\pi$  as the inlet pressure of 40 pounds per square inch. For model 2,  $p_s=570$  pounds per square inch. The angular scale  $\theta$  coincides with that used in the experiment because the Sommerfeld solution places the load line at  $\theta=90^{\circ}$ .

#### EXPERIMENTS BY MCKEE AND MCKEE

Eight cases of experimental pressure distributions in bearings of  $l/d=1.15$  under normal central load are presented by McKee and McKee in reference 11. Four of the experiments were conducted on a journal bearing having a diametral clearance of 0.005 inch and four, on a bearing having 0.002-inch clearance. Both bearings were 1.00 inch long and 0.87 inch in diameter. Maximum applied loads were 25 pounds and the maximum journal speed was 592 rpm. The bearings were operated completely submerged in the lubricating oil, and the temperature of the oil was measured with a thermometer located in the oil bath several inches from the bearing film.

In figure 10, a comparison is made of the experimental distributions with those given by the short-bearing function for the four tests with the diametral clearance of 0.005 inch. The agreement between experiment and theory was better for these tests than for those with 0.002-inch diametral clearance. Calculations of capacity number, eccentricity ratio, pressure distribution, attitude angle, peak-pressure angle, and peak-pressure ratio were made in the same manner as for model 2. Some of the analytical and experimental quantities are compared in the table below.

The experimental values of peak-pressure ratio and peak-pressure angle for both clearances are compared with the short-bearing analytical curves in figures 11 and 12. It may be seen that the agreement between experiment and theory is not so close for the 0.002-inch clearance as for the larger clearance. In figure 10 it may be seen that the divergence of the experimental and analytical pressures is such that the analytical values represent an average of the experimental values which are in some instances above and in some instances below the analytical ones.

Although the comparisons of the analytical quantities with those by McKee and McKee are not so close as those with model 2, it may be seen from figure 10 that the agreement is reasonable as to order of magnitude of pressures and the shape of the pressure-distribution curves.

Quantity	Test 1		Test 2		Test 3		Test 4	
	Experimental	Analytical	Experimental	Analytical	Experimental	Analytical	Experimental	Analytical
Capacity number, $C_s$ .....	-----	0.0815	-----	0.0785	-----	0.0300	-----	0.0352
Eccentricity ratio, $n$ .....	-----	0.555	-----	0.561	-----	0.713	-----	0.688
Attitude angle, $\phi$ , deg.....	50	50	48	49	52	37	51 $\frac{1}{2}$	39
Peak-pressure angle, $\alpha$ , deg.....	12 $\frac{1}{2}$	18 $\frac{1}{2}$	12	18 $\frac{1}{2}$	18	15	15	16
Peak-pressure ratio, $k$ .....	3.06	3.00	3.13	3.00	3.79	3.83	2.83	3.63

\* Analytical value of  $\phi$  is measured from load line to location of zero pressure which theoretically coincides with minimum film thickness.

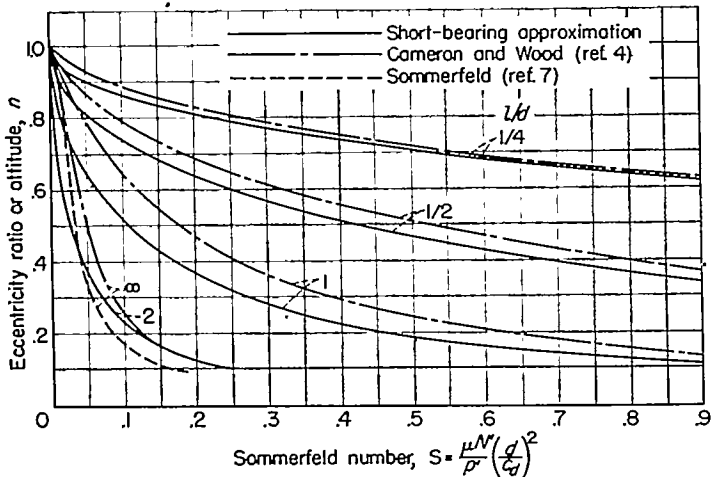


FIGURE 33.—Eccentricity ratio plotted against Sommerfeld number for comparison of analytical curves.

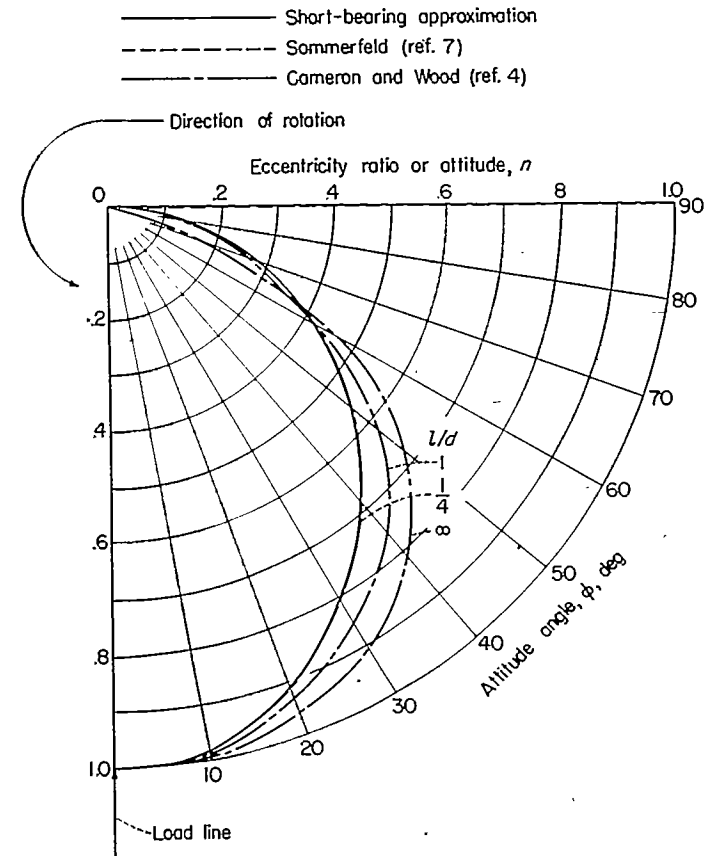


FIGURE 34.—Eccentricity ratio plotted against attitude angle for comparison of analytical curves.

It is interesting to note that the region of pressures below atmospheric as shown experimentally is small enough to be considered negligible as is assumed in the short-bearing approximation.

#### COMPARISON WITH OTHER ANALYTICAL SOLUTIONS

In both the analytical work of Cameron and Wood (ref. 4) and in the short-bearing approximation of this report, length-diameter ratio has been incorporated as an important variable in journal-bearing performance. For this reason, a comparison is made in figures 33 to 35 of curves of eccentricity ratio, attitude angle, and friction variable as given by these analytical solutions. In addition, analytical curves determined by Sommerfeld (ref. 7) for bearings without endwise flow are also shown for comparison.

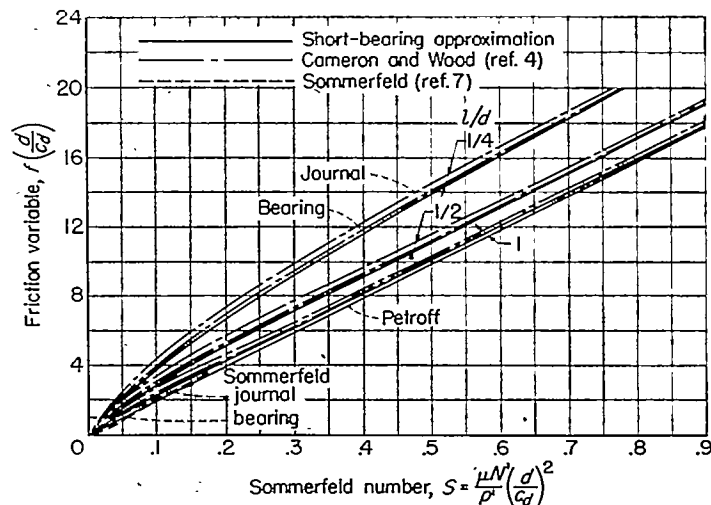


FIGURE 35.—Friction variable plotted against Sommerfeld number for comparison of analytical curves.

The differences in the analytical solutions lie in the basic assumptions made in each case. Both the solution by Cameron and Wood and the short-bearing approximation assume a 180° ruptured film, differing from the Sommerfeld solution which assumes a continuous film of 360°. This difference is of great influence as shown in the curves of eccentricity ratio and attitude angle in figures 33 and 34; the curves representing the two analytical solutions assuming ruptured films are in reasonably good agreement but are quite divergent from the solution depending upon a continuous film.

An important difference between the solution by Cameron and Wood and the short-bearing solution is that the former is based on a ruptured film whose extent depends upon the Sommerfeld number, and the latter assumes that the ruptured film extends 180° for all values of the Sommerfeld number. Another important difference is that the solution by Cameron and Wood is exact mathematically in satisfying Reynolds' equation (eq. (1)) whereas the short-bearing solution is not because of the assumption of a linear velocity profile in the circumferential direction of fluid flow. It is interesting to note that the two solutions for eccentricity ratio and attitude angle are less divergent as  $l/d$  becomes smaller and approach each other as  $l/d$  approaches zero.

The Sommerfeld solution crosses the lines for the short-bearing solution, as shown in figure 33, giving lower values of eccentricity ratio at light loads and higher eccentricity ratios than the short-bearing solution in the heavily loaded region of low Sommerfeld numbers. Apparently the Sommerfeld curve and the curves plotted from Cameron and Wood points for  $l/d = \infty$  do not intersect as is indicated by the two curves in figure 33.

Figure 35 compares friction variable as given by the three analytical solutions. Again the theory of Cameron and Wood and the short-bearing theory are in close agreement

on the effect of  $l/d$  ratios. Because the solution by Cameron and Wood satisfies Reynolds' equation, it shows a difference in friction variable for the bearing and for the journal as shown in figure 35; the short-bearing solution does not indicate this difference because of the assumed linear circumferential film velocity profile. For an  $l/d$  greater than 1.0, all solutions are well approximated by the Petroff line at the high Sommerfeld numbers. It is interesting that all solutions assume a 360° film in determining the friction variable. Apparently this assumption is valid from experimental results.

An important feature of the Sommerfeld solution and the short-bearing solution is that the solutions appear in equation form giving simple relationships among the bearing variables in nondimensional quantities.

#### ANALYSIS AND DISCUSSION

Figures 13 to 19 represent the principal results of this investigation and include only the experimental data for bearings of  $l/d$  ratios of 1,  $\frac{1}{2}$ , and  $\frac{1}{4}$ . All these data are in useful agreement with the theoretical analysis. The data for bearings of  $l/d=2$  which were not in satisfactory agreement as shown in reference 17 are not included. One of the simplifying assumptions limits the theoretical analysis to bearings of short length, and it would be expected that the most satisfactory agreement with experiment would be in the low  $l/d$  range. A relatively small amount of data were taken at  $l/d=2$  at a single speed of 500 rpm. The important techniques of determining the position of zero eccentricity, of taking data at increasing and decreasing increments of load, and of waiting for the condition of thermal equilibrium were developed after the curves for  $l/d=2$  were available for study and were used in tests at  $l/d=1$ ,  $\frac{1}{2}$ , and  $\frac{1}{4}$ . Conclusions in regard to application of the short-bearing approximation above  $l/d=1$  should be withheld until more data are available.

#### ECCENTRICITY RATIO

Although the data shown in figures 14 and 15 for journal eccentricity are considered to be in good agreement with theory, the line through the experimental data lies slightly above the theoretical line. Four factors which may have contributed to this discrepancy are apparent.

First, the effect of inlet oil pressure is to raise the experimental curve at low values of  $n$ . The inlet oil pressure apparently acts on sufficient area of the bearing surface to cause a load adding to the external load. The effect of inlet oil pressure is usually of minor importance because the effect of inlet oil pressure is relatively less with increasing load and also because the value of  $n$  is not critical for bearings with light load or large capacity numbers.

Second, disregarding machining imperfections of the parts, the bending deflection of the shaft under load caused a departure from the ideal shape, especially in the long journals. At  $l/d=1$ , the journal itself was deflected to a parabolic shape; in the case of the double journals of  $l/d=\frac{1}{2}$  and  $\frac{1}{4}$ , the journals were too short to be greatly bent, but, because the journals were located to each side of the center of the load,

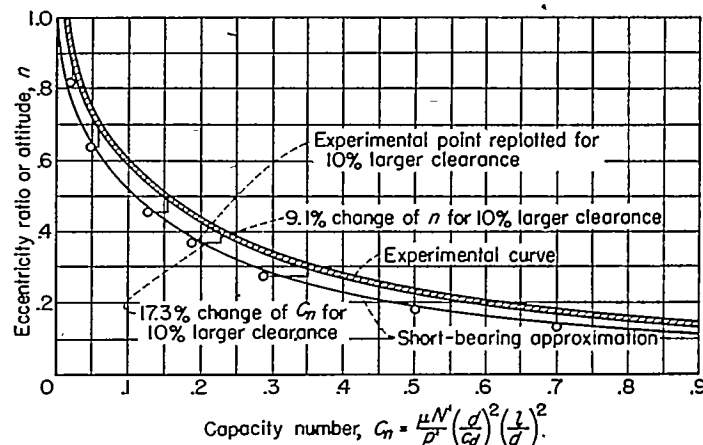


FIGURE 36.—Effect of error in bearing clearance measurement on eccentricity ratio and capacity number. Shown is amount which experimental curve changes based on assumption that actual clearance of bearing is 10 percent larger than clearance measured by "play" method.

their axes were tilted with respect to the bearing axis. Thus, the experimental curve represents the average location of a deflected journal for comparison with an ideal condition.

Third, the magnitude of the clearance both at room temperature and at elevated temperature is of major importance in calculating eccentricity ratio. An error of 0.0001 inch in the radial clearance would represent an error of nearly 10 percent of  $n$  and is proportional to  $n$ . Although the method of measuring clearance by the play of the journal in the bearing is considered the most accurate method, it is the minimum clearance that is measured in this manner to the exclusion of the valleys which may exist in the bearing. The actual average clearance is evidently greater if the valleys are included.

Fourth, the short-bearing approximation neglects the effect of film pressure on the leakage flow in the circumferential direction so that the experimental points should have a slightly greater eccentricity than the theoretical curve. However, as shown in figures 14 and 15, the data for both  $l/d=1$  and  $l/d=\frac{1}{4}$  were closer to the theoretical line than those for  $l/d=\frac{1}{2}$ , showing the experimental spread.

It is suggested that the experimental lines in figures 14 and 15 be used in place of the theoretical line to be on the safe side. In practice the clearance is usually stated as a tolerance, and the effects of wear and thermal changes of clearance and viscosity must also be considered.

As shown in figure 36, the location of the experimental curve is very sensitive to an error in clearance. A 10-percent increase in clearance would lower the experimental line about 9 percent of  $n$  and also move the value of the capacity number to the left by about 17 percent since the clearance term is squared. If the data were recalculated assuming a radial clearance 10 percent larger, the experimental line would fall almost exactly on the theoretical line. The recalculated line would then pass through the point  $n=1.00$  and  $C_n=0$ . Certainly the shaft touches the bearing when the load is high and the speed is zero, that is,  $n=1.00$  when  $C_n=0$ . With a 10-percent increase in clearance, the spread of the data in figure 14 would remain almost unchanged, but the maximum

value of  $n$  reached by the data would fall from about 0.99 to 0.90. With the data ending at  $n=0.90$  the line could easily be faired through the point  $n=1.00$  at  $C_n=0$ . It should also be noticed that a 5-percent increase in clearance would also permit fairing the curve across a similar gap between  $n \approx 0.95$  and  $n=1.00$ .

#### FRICITION

Two methods of plotting the same friction data are shown for comparison in figures 16 and 17. The common method of plotting friction consists in plotting numbers containing the friction coefficient  $f$  on the vertical axis against the Sommerfeld number  $S$  or capacity number  $C_n$  on the horizontal axis as shown in figure 16. This results in a line which falls toward the origin with increasing load, rising abruptly if metallic contact begins. The use of the friction coefficient has been described as misleading by several authors in that the friction coefficient increases directly with  $S$  or  $C_n$ , leading to the thought that there are large changes in friction or friction torque with comparable changes in load. Another difficulty with this kind of plotting is that the values of the friction coefficient are difficult to read in the interesting region of high load since the data plot so near the origin.

To avoid the above difficulties, the friction data are plotted in the manner shown in figure 17 which consists of plotting the ratio of the frictional force at the bearing surface to the Petroff no-load friction against the load number. This gives the frictional force variations in direct relation to load. It is to be noted that figure 17 shows the spread of the experimental data more clearly, whereas the small spread at the low end of the curve on figure 16 actually has the same percent of spread.

Figure 17 permits a direct and easy prediction of friction torque, eliminating the use of the friction coefficient. Figure 17 gives the percent increase of friction under load to be applied to the well-known Petroff friction at no load which introduces the main factors on which the friction depends.

It is interesting to note that, although the analysis is concerned principally with the loaded  $180^\circ$  of the bearing, it arrives at the friction force by an integration of the shearing stresses in the oil film over the full  $360^\circ$ . The experimental data indicate that such a view of the extent of the oil film is acceptable for estimating friction. This also bears out the view of Cameron and Wood (ref. 4) that the cavitated film on the unloaded side of the bearing behaves as an uncavitated film in laminar flow insofar as friction is concerned. There is a possibility that the cool entering oil compensates for the effects of cavitation.

At near zero load high inlet pressure produced values of the friction which were considerably higher than the theoretical values. This may be associated with an internal load caused by high inlet oil pressure as indicated in figure 17.

Theoretically, the short-bearing approximation can make no distinction between bearing friction and journal friction inasmuch as the velocity profile in the oil film is assumed to be linear in the circumferential direction. Actually, a difference is thought to exist which depends upon the couple equal to  $P_e \sin \phi$  as already discussed.

#### OIL FLOW

Two distinct nondimensional terms have been used for plotting the oil flow results, the oil number  $q_n$  (fig. 18) and the oil flow factor  $q$  (fig. 19). Although the oil flow number used in figure 18 can be obtained analytically, a nondimensional number similar to this was suggested by Blok in the discussion of the paper by Cameron and Wood (ref. 4).

As shown in figure 18, there is considerable variation of the oil flow number, both above and below the line representing theoretically required flow. Figure 19 is the result of plotting the ratio of total oil flow to the theoretical flow, called oil flow factor  $q$ , against the inlet-pressure capacity number. While there is some spread of the points at the center of the curve, the grouping of the points, especially at the ends, is an invitation to draw a single line. It should not be overlooked that one of the points is nearly 100 percent off the single-line curve, but there is a possibility of experimental error in the more divergent points since the two worst points are from a single run. This curve permits the total flow to be predicted for any of the test runs.

The flow issuing from the ends of the bearing in the  $180^\circ$  of the converging film is equal to the difference between the amount of oil entering the wedge and that leaving the wedge to circulate again. The difference also equals the amount of oil flow theoretically required to maintain the converging wedge full. This amount is only a part of the total flow of the bearing as measured experimentally, assuming the surplus flow is positive. The diverging wedge is an area of low pressure in the oil film, and, if oil is present at the ends of the bearing, the flow may be inward. However, if the oil inlet pressure is sufficient, the flow from the  $180^\circ$  of the diverging wedge will be positive, and it can be called the surplus flow whatever its sign.

#### OIL FLOW STARVATION

In figure 18, some of the points representing the experimental oil flow fall below the theoretically required oil flow line. This is also shown in figure 19 by all points having a flow factor less than 1 or an inlet pressure capacity number greater than 0.12. This amount of oil flow can have either of two meanings. First, a condition that can be called starvation is occurring if the flow entering the converging wedge is less than that theoretically required. The second possibility is that the surplus flow is negative, which would mean that oil is available around the ends of the bearing and is being drawn into the low-pressure area, thus adding to the supply of oil for the converging wedge. In some test machines a bead of oil can be seen around the ends of the bearing at low rotative speeds, while at higher speeds the bead of oil is thrown clear.

When starvation actually occurs, it would apparently mean that the film thickness at the entrance of the converging wedge is not completely filled over the full length of the bearing. As the oil flows through the wedge, it can be imagined as spreading out leaving the entering corners unfilled. These are in a low-pressure region of the oil film where the lack of oil would cause the least effect on the total load capac-

ity. There is a possibility that this condition of oil starvation is fairly common at the higher rotative speeds if a single oil hole is used without oil grooves.

In passing, it may be of interest to note that the denominator of the ratio denoting the oil flow number has some physical significance. The denominator of the oil flow number is equal to the theoretical flow of a bearing for the special case when  $n=1$ , that is, when the journal is touching the bearing.

The oil flow curves strictly apply only to the bearing under test, having a small oil inlet hole without grooves. The oil flow data given by McKee (ref. 14) are in excellent agreement for the single-oil-hole case and show the increase in oil flow obtained by an axial oil inlet groove. Figure 19 particularly has the interesting possibility of applying to bearings of other diameters.

#### USE OF CURVES

Figures 15, 17, and 19 may be used as charts to facilitate rapid determination of the performance characteristics of a bearing if the various items in the load number and inlet oil pressure are known. The bearing clearance should be corrected for thermal expansion. Upper and lower limits of bearing clearance may be used to simulate production tolerances and wear. The viscosity desired is that of the oil film and was approximated in these experiments from temperature readings of thermocouples embedded near the bearing surface in the loaded area. If possible, the oil flow should be measured to determine a factor to be applied to the values of figure 19 to allow for the effects of variations of oil grooving, which have not been determined experimentally in this report.

If the operating temperature is known, the charts can be used to estimate the operating conditions. The charts are particularly useful to estimate the effects of various changes on the bearing. Changes which affect the operating temperature, such as alteration of viscosity, oil flow, clearance, or speed, require an approximation of the new equilibrium temperature. The charts may be used on a new design, where the bearing operating temperature is unknown, to determine values at two or more arbitrary temperatures representing an allowable temperature range.

#### HEAT-BALANCE DIAGRAM

The construction of a heat-balance diagram as suggested in figure 37 is aided considerably if an operating temperature at a different set of conditions is already known, since some of the unknowns can then be determined. The temperature of a bearing will stabilize at a point where the heat generated balances the heat lost to the oil flow plus the heat lost by other means such as conduction, radiation, and convection. If calculations are made at two or more arbitrary temperatures, a graphical solution similar to figure 37 can then be made of heat generated and heat loss against assumed temperature. A few points of the line representing other heat losses will be needed. These points can be obtained from similar graphs on the same application for conditions where the temperature is known. The equilibrium temperature of the bearing will be indicated by the point of

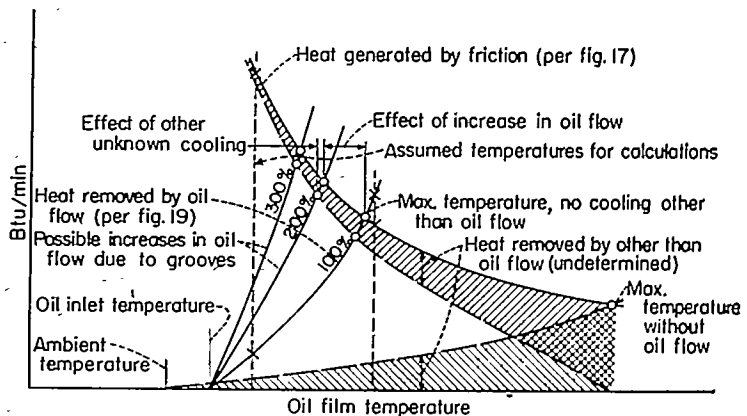


FIGURE 37.—Heat-balance curves for estimating equilibrium oil film temperature.

intersection of the heat-generated and heat-dissipated lines on this graph as illustrated in figure 37.

In high-speed, high-load applications where the ambient temperature is high, it may be acceptable to assume that a high percentage of the heat is transferred to the oil. In this case, the intersection point represents a limiting or maximum temperature which will be reduced slightly by the remaining cooling. The heat-balance diagram shows the relative effect of various assumed changes on bearing temperature, and a useful approximation of bearing temperature can often be reached even if complete information is lacking.

#### HEAT GENERATED BY FRICTION AND POWER LOSS

As already discussed, the couple caused by the eccentricity of the load should theoretically be added to the bearing-friction torque to give the journal-friction torque. If the bearing is stationary, it is the journal-friction torque which should be used in estimating the rate of heat generation and power loss. The data for computing the additional friction due to the horizontal eccentricity ratio  $n_h$  are given in figure 13.

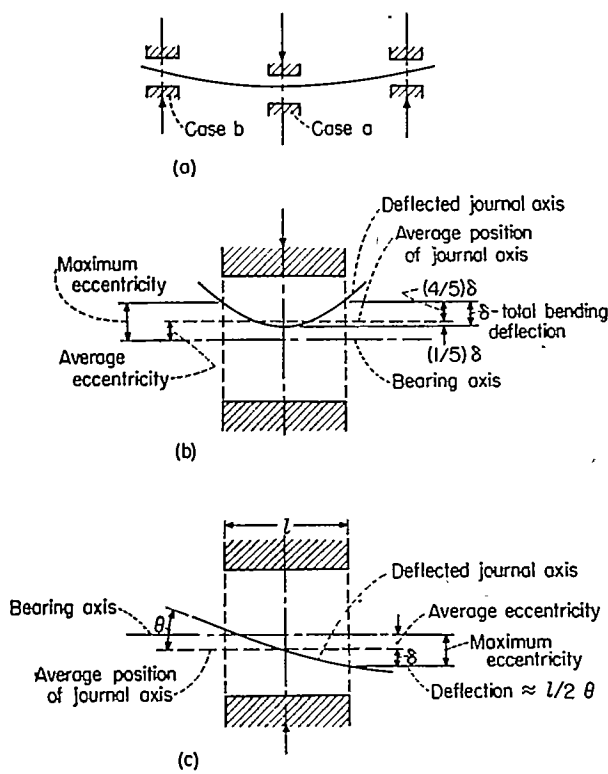
#### HEAT REMOVED BY OIL FLOW

The heat removed by the oil flow is equal to the temperature rise times the flow rate in pounds per minute times the specific heat of the oil. The oil flow estimated, using the oil flow factor from figure 19, would be increased if oil grooves were present. Some data on the increase are given by McKee (fig. 19) and by Clayton (ref. 18). Some experimental data on the actual bearing or a similar bearing would be valuable.

#### MAXIMUM ECCENTRICITY AT ENDS OF A BEARING

After the operating temperature of a bearing has been determined by actual measurement, or by estimating it by means of the heat-balance graph, the eccentricity ratio of a theoretically straight shaft may be obtained from figure 14 or 15. Corrections may then be applied to estimate the maximum eccentricity ratio at the ends of the bearing under actual conditions.

In figures 14 and 15 either the experimental line or the theoretical line may be used for predicting values of  $n$ . The experimental line gives values of  $n$  which are about 10 percent



(a) Position of bearing in relation to journal for cases a and b.  
 (b) Case a, journal axis parallel to bearing axis at center of bearing.  
 (c) Case b, journal axis inclined to bearing axis at center of bearing.

FIGURE 38.—Effect of deflection and misalignment on eccentricity at ends of bearing.

higher than those of the theoretical line and which would be on the safe side. The higher values were based on clearance measured by the play method which reads the minimum clearance between the high spots on the shaft and the bearing. If clearances in production are measured by ring and plug gages, the eccentricity ratio might be nearly comparable with the experimental data.

The theoretical line in figure 14 or 15 may be used by altering the value of the eccentricity to allow for hills and valleys or waviness in the surface. For example, if this inaccuracy is 0.0001 inch in a bearing having  $c_r = 0.001$  inch, the allowance to be added is equivalent to an  $n$  value of one-ninth of  $n$ .

The following considerations should be included in estimating the eccentricity ratio in an actual bearing:

(1) The clearance at operating temperature is often considerably altered from that at room temperature, and the plotted data are based on clearance at operating temperature.

(2) If the bearing is to be operated at very light load the effect of additional load due to inlet oil pressure becomes appreciable.

(3) The radius of curvature of the shaft should be estimated and the deflection at the ends of the bearing computed relative to the center. The deflection can then be converted to an  $n$  value by dividing by the radial clearance and the result added to the chart value of  $n$ . Two cases arise (see fig. 38):

(a) If the bearing axis and the journal axis are parallel at the center of the bearing, four-fifths of the deflection should be converted to an  $n$  value and added to the chart value of  $n$ . Assuming that the deflection curve is a fourth-degree parabola, the eccentricity ratio will be decreased one-fifth at the center and increased four-fifths at the ends, which corresponds to the method used in obtaining the curves.

(b) If the journal axis is at an angle to the bearing axis at the bearing center, the slope of the deflection curve will give a change in displacement from the center to one end. The full value of this figure should be converted to an  $n$  value and added to the chart value of  $n$  to correspond to the method used in obtaining the charts.

(4) Similar methods of estimating the increase in eccentricity ratio at the ends of the bearing should be applied for misalignment caused by differences in thermal expansion of the bearing supports and for machining or assembly tolerances. If possible the bearing supports should be designed so that their deflection counteracts the deflection of the shaft, and a correction for this can be introduced.

The resulting estimated eccentricity ratio at the ends of the bearing is a point considerably above the chart value shown by figure 14 or 15. A series of similar points at different loads would give a line representing  $n$  at the ends of the bearing comparable with the theoretical curve. The difference in eccentricity ratio between the center and the ends of the bearing increases with bearing length and decreases with an increase in bearing clearance.

It should be noted that the above procedure for determining the eccentricity ratio at the end of a bearing constitutes a quantitative method for evaluation of the effect of misalignment on a bearing, if the angle is known.

#### PRACTICAL LIMITS OF ECCENTRICITY RATIO

The operating limit of a bearing is evidently determined by the maximum value of the eccentricity ratio at any point within the bearing, and, if the bearing and journal are true cylinders, this occurs at the ends of the bearing. Soft bearing materials will evidently wear-in or accommodate themselves to a stable running condition, the bearing surface then becoming a curved surface similar to the deflected journal surface. In this case it is the change in deflection with a sudden increase in load which becomes important rather than the total deflection. However, if the eccentricity at the ends allows a suitable reserve of  $n$  value for overload, grit in the oil, machining and thermal variations, and so forth, little difficulty or wear should occur during running. Practical values of  $n$  can best be determined by comparison with values from well-proven designs of a similar character.

It is probable, although it has not been investigated experimentally, that a correlation exists between the eccentricity at the ends of the bearing as predicted above and the operating conditions at the point of the hook in friction curves. It has already been found using an earlier babbitt bearing in the machine used in the present investigation that the hook point will progress toward more severe conditions with continued running, the first hook possibly being of a very short

duration. This is an example of the ability of babbitt to conform to a deflected journal, a sudden change in deflection causing a temporary hook point.

#### MEANING OF LOAD NUMBER

The load number or the capacity number can be written in several different forms by manipulating the arrangement of the terms. In the expression for  $C_n$ , canceling the diameter term in numerator and denominator gives one interesting expression

$$C_n = \frac{\mu N'}{p'} \left( \frac{d}{c_d} \right)^2 \left( \frac{l}{d} \right)^2 = \frac{\mu N'}{p'} \frac{l^2}{c_d^2} \quad (34)$$

and substituting the total load  $P$  over  $ld$  for the unit load on projected area  $p'$  produces other forms:

$$C_n = \frac{\mu N'}{P} \left( \frac{d}{c_d^2} \right) l^2 = \frac{\mu N'}{P} \left( \frac{\sqrt{d}}{c_d} \right)^2 l^3 \quad (35)$$

All of the relations are limited to the range of  $l/d$  from  $\frac{1}{4}$  to 1 which have thus far been investigated experimentally. The range in which these relations are true is also considerably limited by the increased deflection of a smaller diameter. Perhaps the most important consideration neglected in these theoretical relations is the effect on viscosity that might result from a change in the bearing temperature.

Equation (34) indicates that the capacity number and the eccentricity ratio of a given bearing are independent of bearing diameter if the unit loading and the bearing clearance are held constant. This is to be interpreted to mean that, for a small increase in diameter, the bearing clearance must be constant if the increased bearing area at the same unit bearing loading is to be taken advantage of. Large increases in diameter usually require some increase in bearing clearance for thermal expansion or contraction.

Equation (35) indicates that the capacity number and the eccentricity ratio of a bearing are independent of the diameter if the bearing clearance is made proportional to the square root of the diameter, the total load being constant. This rate of increase in clearance may approximate manufacturing requirements in some instances.

Rearranging the terms in equation (35),

$$P = \frac{\mu N'}{C_n} \left( \frac{d}{c_d} \right)^2 \frac{l^3}{d} \quad (36)$$

$$P = \frac{\mu N'}{C_n} \left( \frac{d}{c_d} \right) \frac{l^3}{c_d} \quad (37)$$

Equation (36) indicates that if a constant ratio of diameter to clearance is maintained the total load is inversely proportional to the *diameter* if the capacity number and other variables are constant.

Equation (37) indicates that if a constant ratio of diameter to clearance is maintained the total load is inversely proportional to the *clearance* if the capacity number and other variables are constant.

The verbal statements for both equations (36) and (37) are identical except for the change of the italicized words,

where diameter is exchanged for clearance. It is to be noted that a proportionality has been assumed to exist between the two factors.

It may be hard to believe that the total load varies inversely as the diameter at a constant clearance ratio, but the area can be considered to increase as the first power of the diameter in the numerator, while the  $l/d$  term changes as the second power of the diameter in the denominator. Holding the capacity number and  $n$  constant with increasing diameter may be unnecessarily severe, since this results in an increase in minimum oil film thickness if the clearance ratio is constant.

Equations (34) and (35) indicate that the unit load is proportional to  $l^2$  and the total load, to  $l^3$  for a given capacity number, if other variables are constant.

#### CIRCUMFERENTIAL OIL GROOVES

The effect of a single circumferential oil groove around the center of a bearing may be analyzed by the use of the above equations. Circumferential oil grooves are occasionally used to prevent the scratching which may be caused by abrasive grit lodged in the edge of a simple oil inlet hole.

**Case I.**—Consider a bearing of  $l/d$  of 1 or less with a narrow oil groove  $360^\circ$  around the bearing in the center so that it becomes two bearings side by side. Referring to equation (34), if the area of the oil groove is neglected, the unit load  $p'$  is the same in each case. The  $l/d$  ratio is one-half its former value, and  $\mu$ ,  $N'$ , and  $c_d$  are constant. Therefore,  $C_n$  for the bearing with an oil groove is one-fourth its former value. This means that the effect of the oil groove on eccentricity ratio and oil film thickness would be similar to increasing the load four times. To eliminate uncertainty in regard to a two-to-one error in the above, the result may be checked by a form of the equation including the total load  $P$  such as equation (35). For the bearing with the oil groove each half carries half the load, or  $P/2$ :

$$C_n = \frac{\mu N'}{P} \frac{d}{c_d^2} \left( \frac{l}{2} \right)^3 = \text{One-fourth of original value}$$

**Case II.**—If the original bearing had an  $l/d$  ratio of 2 or more, so that each half had  $l/d > 1$ , these equations would not apply. In this case, a central oil groove is less harmful and may be beneficial by increasing oil flow and resistance to scratching.

#### CONCLUSIONS

The following conclusions may be drawn from the results of the investigation of a short-bearing approximation for full journal bearings:

1. The short-bearing approximation yields equations which give simplified relationships among the bearing variables, yielding single line curves when plotted against the non-dimensional load number.

2. The short-bearing approximation and the Sommerfeld equations for long bearings may be considered as similar types of solution based on different assumptions, and each has a range of length-diameter ratios in which it is useful.

3. After correction for shaft-deflection and bearing-clearance changes at running temperature, the experimental data obtained at length-diameter ratios of 1,  $\frac{1}{2}$ , and  $\frac{1}{4}$  on a 1% inch-diameter bearing are in good agreement with the short-bearing theory. Conclusions in regard to a length-diameter ratio of 2 should be withheld until additional data are available.

4. The elastic deflection of the shaft has a considerable effect on the eccentricity ratio at high loads and increases the eccentricity ratio at the ends of the bearing.

5. The method of predicting eccentricity ratio at the ends of a bearing constitutes a method for quantitative evaluation of the effect of angular misalignment and elastic deflection on full journal bearings.

6. The experimental curves establish the use of the load number as a basic nondimensional variable for plain bearings whose length-diameter ratio is equal to or less than 1. The reciprocal of the load number is equal to the Sommerfeld number times the square of the length-diameter ratio.

7. The form of the load number indicates that in the range of length-diameter ratios of 1 or less and neglecting deflection and temperature changes:

(a) The eccentricity ratio is independent of diameter if the running clearance varies as the square root of the diameter, the total load being constant

(b) The eccentricity ratio is independent of diameter if the unit load and the running clearance are constant

(c) The total load capacity varies inversely with either the diameter or the clearance if the diameter-clearance ratio and the eccentricity ratio are constant

(d) The unit load varies as the length squared and the total load, as the length cubed for constant values of load number and other variables

8. The plot of friction ratio against load number shows the increase of friction with load as a single line, in relation to the friction at no load.

9. The oil flow characteristics of a bearing are reduced to a single-line function of oil flow factor against inlet-pressure capacity number for bearings whose length-diameter ratio is 1 or less.

CORNELL UNIVERSITY,  
ITHACA, N. Y., June 12, 1953.

## APPENDIX

### INTEGRATIONS OF TRIGONOMETRIC FUNCTIONS IN EQUATIONS (14) AND (14a)

For equation (14):

$$\int_0^\pi \frac{n \sin \theta \cos \theta d\theta}{(1+n \cos \theta)^3} = \int_0^\pi \frac{\cos \theta}{(1+n \cos \theta)} \times \frac{n \sin \theta d\theta}{(1+n \cos \theta)^2}$$

Substituting

$$\frac{\cos \theta}{(1+n \cos \theta)} = \frac{1}{n} - \frac{1}{n(1+n \cos \theta)}$$

then

$$\begin{aligned} & \int_0^\pi \left[ \frac{1}{n} - \frac{1}{n(1+n \cos \theta)} \right] \frac{n \sin \theta d\theta}{(1+n \cos \theta)^2} \\ &= -\frac{1}{n} \int_0^\pi \frac{-n \sin \theta d\theta}{(1+n \cos \theta)^2} + \frac{1}{n} \int_0^\pi \frac{-n \sin \theta d\theta}{(1+n \cos \theta)^3} \\ &= \left[ \frac{1}{n(1+n \cos \theta)} \right]_0^\pi - \left[ \frac{1}{2n(1+n \cos \theta)^2} \right]_0^\pi \\ &= \frac{1}{n} \left[ \frac{1}{(1-n)} - \frac{1}{(1+n)} \right] - \frac{1}{2n} \left[ \frac{1}{(1-n)^2} - \frac{1}{(1+n)^2} \right] \\ &= -\frac{2n^2}{(1-n^2)^2} \end{aligned}$$

For equation (14a):

$$\int_0^\pi \frac{n \sin^2 \theta d\theta}{(1+n \cos \theta)^3} = - \int_0^\pi \sin \theta \times \frac{-n \sin \theta d\theta}{(1+n \cos \theta)^2}$$

By using

$$u = \sin \theta$$

$$du = \cos \theta d\theta$$

$$dv = \frac{-n \sin \theta d\theta}{(1+n \cos \theta)^3}$$

$$v = -\frac{1}{2(1+n \cos \theta)^2}$$

and if

$$\left[ \frac{\sin \theta}{2(1+n \cos \theta)^2} \right]_0^\pi = 0$$

then

$$\begin{aligned} & \left[ \frac{\sin \theta}{2(1+n \cos \theta)^2} \right]_0^\pi - \frac{1}{2} \int_0^\pi \frac{\cos \theta d\theta}{(1+n \cos \theta)^2} \\ &= -\frac{1}{2} \int_0^\pi \frac{\cos \theta d\theta}{(1+n \cos \theta)^2} \\ &= -\frac{1}{2} \int_0^\pi \left[ \frac{1}{n} - \frac{1}{n(1+n \cos \theta)} \right] \frac{d\theta}{(1+n \cos \theta)} \\ &= -\frac{1}{2n} \int_0^\pi \frac{d\theta}{(1+n \cos \theta)} + \frac{1}{2n} \int_0^\pi \frac{d\theta}{(1+n \cos \theta)^2} \end{aligned}$$

Using Sommerfeld's substitutions

$$d\theta = \frac{(1-n^2)^{1/2}}{(1-n \cos \alpha)} d\alpha$$

and

$$1+n \cos \theta = \frac{1-n^2}{(1-n \cos \alpha)}$$

then

$$\begin{aligned}
 & -\frac{1}{2n} \int_0^\pi \frac{(1-n^2)^{1/2} d\alpha}{(1-n \cos \alpha)} \times \frac{(1-n \cos \alpha)}{(1-n^2)} + \\
 & \frac{1}{2n} \int_0^\pi \frac{(1-n^2)^{1/2} d\alpha}{(1-n \cos \alpha)} \times \frac{(1-n \cos \alpha)^2}{(1-n^2)^2} \\
 & = -\frac{1}{2n(1-n^2)^{1/2}} \int_0^\pi d\alpha + \frac{1}{2n(1-n^2)^{3/2}} \int_0^\pi (1-n \cos \alpha) d\alpha \\
 & = \left[ -\frac{\alpha}{2n(1-n^2)^{1/2}} \right]_0^\pi + \frac{1}{2n(1-n^2)^{3/2}} [\alpha - n \sin \alpha]_0^\pi \\
 & = -\frac{\pi}{2n(1-n^2)^{1/2}} + \frac{\pi}{2n(1-n^2)^{3/2}} \\
 & = \frac{\pi n}{2(1-n^2)^{3/2}}
 \end{aligned}$$

#### REFERENCES

1. Reynolds, O.: On the Theory of Lubrication and Its Application to Mr. Beauchamp Tower's Experiments, Including an Experimental Determination of the Viscosity of Olive Oil. Phil. Trans. Roy. Soc. (London), ser. A, vol. 177, 1886, pp. 157-234.
2. Kingsbury, Albert: Problems in Theory of Fluid-Film Lubrication, With Experimental Method of Solution. Trans. A. S. M. E., APM-53-5, vol. 53, 1931, pp. 59-74.
3. Christopherson, D. G.: A New Mathematical Method for the Solution of Film Lubrication Problems. Proc. Institution Mech. Eng. (London), vol. 146, no. 3, 1941, pp. 126-135.
4. Cameron, A., and Wood, W. L.: The Full Journal Bearing. Proc. Institution Mech. Eng. (London), vol. 161, W. E. P. Nos. 47-54, 1949, pp. 59-72.

5. Navier, Claude L. M. H.: Memoir on the Laws of Fluid Motion. Mem., Acad. Sci. (Paris), vol. 6, 1827, p. 389.
6. Stokes, G. G.: On the Theories of the Internal Friction of Fluids in Motion. Trans. Cambridge Phil. Soc., vol. 8, 1845.
7. Sommerfeld, A.: The Hydrodynamic Theory of Lubrication Friction. Zs. Math. und Phys., vol. 50, nos. 1 and 2, 1904, pp. 97-155.
8. Harrison, W. J.: The Hydrodynamical Theory of Lubrication With Special Reference to Air as a Lubricant. Proc. Cambridge Phil. Soc., vol. 22, no. 3, 1913, pp. 39-54.
9. Michell, A. G. M.: Progress in Fluid-Film Lubrication. Trans. A. S. M. E., MSP-51-21, vol. 51, 1929, pp. 153-163.
10. Cardullo, F. E.: Some Practical Deductions From Theory of Lubrication of Short Cylindrical Bearings. Trans. A. S. M. E., MSP-52-12, vol. 52, 1930, pp. 143-153.
11. McKee, S. A., and McKee, T. R.: Pressure Distribution in Oil Films of Journal Bearings. Trans. A. S. M. E., RP-54-8, vol. 54, 1932, pp. 149-165.
12. Bradford, L. J., and Grunder, L. J.: Oil Film Pressures in a Complete Journal Bearing. Eng. Exp. Station Bull. No. 39, Penn. State College Bull., vol. XXIV, no. 40, Sept. 8, 1930, pp. 1-50.
13. Dubois, G. B., Mabie, H. H., and Ocvirk, F. W.: Experimental Investigation of Oil Film Pressure Distribution for Misaligned Plain Bearings. NACA TN 2507, 1951.
14. McKee, S. A.: Oil Flow in Plain Journal Bearings. Preprint, A. S. M. E. Paper No. 51-A-34, Nov. 1951.
15. Bradford, L. J., and Davenport, C. C.: Characteristic Curves for Fluid Film Lubricated Journal Bearings. Refrigerating Eng., vol. 24, Dec. 1932, pp. 343-347.
16. Phelan, R. M.: The Design and Development of a Machine for the Experimental Investigation of Dynamically Loaded Sleeve Bearings. M. M. E. Thesis, Cornell Univ., June 1950.
17. Dubois, G. B., and Ocvirk, F. W.: Experimental Investigation of Eccentricity Ratio, Friction, and Oil Flow of Short Journal Bearings. NACA TN 2809, 1952.
18. Clayton, D.: An Exploratory Study of Oil Grooves. Proc. Institution Mech. Eng. (London), vol. 155, War Emergency Issue No. 14, 1946, pp. 41-49.

TABLE I.—SAMPLE LOG SHEET FOR JOURNAL DISPLACEMENT RUN USING SAE 10 OIL WITH  $l/d = \frac{1}{2}$ ,  $N = 5,000$  RPM, AND  $p_o = 100$  POUNDS PER SQUARE INCH[Bearing diameter,  $1\frac{3}{8}$  in.; length,  $1\frac{1}{4}$  in.; diametral clearance at room temperature, 0.00232 in.; bronze bearing; steel shaft with two journals; oil fed through one  $3/16$ -in.-diam. hole at each journal]

## (a) Counterclockwise shaft rotation

Time	Shaft rotation	Speed, rpm	Capsule pressure, lb/sq in.	Displacement by dials, in.				Temperature (°F) at thermocouple in—												Test oil						
				Left vertical	Right vertical	Left horizontal	Right horizontal	Test bearing		Test bearing		Room temperature by thermometer, °F														
								Left bearing	Right bearing	Block	Loaded side	Unloaded side	Inlet oil	Air												
4:13	COW	5000	4.5	0.00021	-0.00020	-0.00006	-0.00009	152	153	156	153	153	156	157	160	146	149	158	151	156	158	133	85	138	4	
				0.00017	-0.00017	0.00003	0.00004	153	153	156	153	153	156	157	160	147	149	158	151	156	158	133	85	100	100	
				7.5	0.00028	-0.00013	0.00012	0.00023	153	153	156	153	153	156	157	160	147	149	158	151	156	158	133	85	100	100
				10.0	0.00042	-0.00004	0.00018	0.00036	153	153	156	153	153	156	157	160	147	149	158	151	156	158	133	85	100	100
				12.5	0.00050	0.00009	0.00020	0.00040	153	153	156	153	153	156	157	160	147	149	158	151	156	158	133	85	100	100
				15.0	0.00060	0.00017	0.00023	0.00040	153	153	156	153	153	156	157	160	147	149	158	151	156	158	133	85	100	100
				20.0	0.00075	0.00029	0.00022	0.00040	153	153	156	153	153	156	157	160	147	149	158	151	156	158	133	85	100	100
				25.0	0.00083	0.00039	0.00022	0.00040	153	153	156	153	153	156	157	160	147	149	158	151	156	158	133	85	100	100
				30.0	0.00091	0.00049	0.00031	0.00040	153	153	156	153	153	156	157	160	147	149	158	151	156	158	133	85	100	100
				40.0	0.00105	0.00061	0.00020	0.00038	153	153	156	153	153	156	157	160	147	149	158	151	156	158	133	85	100	100
				50.0	0.00113	0.00072	0.00018	0.00035	153	153	156	153	153	156	157	160	147	149	158	151	156	158	133	85	100	100
				60.0	0.00121	0.00080	0.00016	0.00033	153	153	156	153	153	156	157	160	147	149	158	151	156	158	133	85	100	100
				60.0	0.00122	0.00080	0.00016	0.00033	153	153	156	153	153	156	157	160	147	149	158	151	156	158	133	85	100	100
				50.0	0.00116	0.00070	0.00016	0.00034	153	153	156	153	153	156	157	160	147	149	158	151	156	158	133	85	100	100
				40.0	0.00106	0.00059	0.00016	0.00037	153	153	156	153	153	156	157	160	147	149	158	151	156	158	133	85	100	100
				25.0	0.00087	0.00038	0.00019	0.00049	153	153	156	153	153	156	157	160	147	149	158	151	156	158	133	85	100	100
				20.0	0.00074	0.00028	0.00019	0.00040	153	153	156	153	153	156	157	160	147	149	158	151	156	158	133	85	100	100
				16.0	0.00059	0.00016	0.00020	0.00040	153	153	156	153	153	156	157	160	147	149	158	151	156	158	133	85	100	100
				12.5	0.00049	0.00008	0.00020	0.00040	153	153	156	153	153	156	157	160	147	149	158	151	156	158	133	85	100	100
				10.0	0.00042	-0.00005	0.00018	0.00037	153	153	156	153	153	156	157	160	147	149	158	151	156	158	133	85	100	100
				7.5	0.00027	-0.00018	0.00011	0.00023	153	153	156	153	153	156	157	160	147	149	158	151	156	158	133	85	100	100
				4.5	0.00017	-0.00017	0.00004	0.00007	153	153	156	153	153	156	157	160	147	149	158	151	156	158	133	85	100	100
				4.5	0.00021	-0.00020	-0.00005	-0.00006	153	153	156	153	153	156	157	160	147	149	158	151	156	158	133	85	100	100
4:40	COW	5000	4.5	0.00021	-0.00020	-0.00005	-0.00006	153	153	156	153	153	156	157	160	147	149	158	151	156	158	133	85	137	4	

\* COW, counterclockwise.

## (b) Clockwise shaft rotation

Time	Shaft rotation	Speed, rpm	Capsule pressure, lb/sq in.	Displacement by dials, in.				Temperature (°F) at thermocouple in—												Test oil							
				Left vertical	Right vertical	Left horizontal	Right horizontal	Test bearing		Test bearing		Room temperature by thermometer, °F															
								Left bearing	Right bearing	Block	Loaded side	Unloaded side	Inlet oil	Air													
3:05	CW	5000	4.5	0.00005	0.00010	-0.00003	-0.00003	153	159	156	152	155	156	159	144	145	148	157	150	157	160	156	129	84	138	4	
				4.5	0.00002	0.00013	-0.00011	-0.00021	153	159	156	152	155	156	157	144	145	148	157	150	157	160	156	129	84	100	100
				7.5	0.00012	0.00011	-0.00024	-0.00036	153	159	156	152	155	156	157	144	145	148	157	150	157	160	156	129	84	100	100
				10.0	0.00028	0.00015	-0.00033	-0.00051	153	159	156	152	155	156	157	144	145	148	157	150	157	160	156	129	84	100	100
				12.5	0.00041	0.00023	-0.00040	-0.00060	153	159	156	152	155	156	157	144	145	148	157	150	157	160	156	129	84	100	100
				15.0	0.00047	0.00038	-0.00041	-0.00062	153	159	156	152	155	156	157	144	145	148	157	150	157	160	156	129	84	100	100
				20.0	0.00062	0.00052	-0.00045	-0.00062	153	159	156	152	155	156	157	144	145	148	157	150	157	160	156	129	84	100	100
				25.0	0.00074	0.00055	-0.00045	-0.00062	153	159	156	152	155	156	157	144	145	148	157	150	157	160	156	129	84	100	100
				30.0	0.00082	0.00057	-0.00044	-0.00060	153	159	156	152	155	156	157	144	145	148	157	150	157	160	156	129	84	100	100
				40.0	0.00094	0.00082	-0.00044	-0.00058	153	159	156	152	155	156	157	144	145	148	157	150	157	160	156	129	84	100	100
				50.0	0.00106	0.00092	-0.00043	-0.00062	153	159	156	152	155	156	157	144	145	148	157	150	157	160	156	129	84	100	100
				60.0	0.00112	0.00097	-0.00043	-0.00064	153	159	156	152	155	156	157	144	145	148	157	150	157	160	156	1			

TABLE II.—SAMPLE LOG SHEET FOR FRICTION AND OIL FLOW RUN USING SAE 10 OIL WITH  $4d=1$ ,  $N=1,000$  RPM, AND  $p_o=100$  POUNDS PER SQUARE INCH[Bearing diameter,  $1\frac{3}{16}$  in.; length,  $1\frac{3}{16}$  in.; diametral clearance at room temperature, 0.00264 in.; bronze bearing; steel journal; oil fed through one  $\frac{1}{16}$ -in.-diam. hole]

Time	Shaft rotation	Speed, rpm	Cap- sule pres- sure, lb/sq in.	Manometer reading, in. of Hg	Cal- ibration torque, in-lb	Temperature (°F) at thermocouple in—																Test oil	Oil flow					
						Left bearing		Test bearing								Right bearing		Test bearing				Room temperature by ther- mometer, °F						
						0	1	2	3	4	5	6	7	8	9	10	11	12	13	14	15	16	24					
3:15	COW	1000	3.0	11.00	11.72	-0.72	107	122	122	122	122	122	122	106	118	122	122	122	120	120	110	78	78	130	100	0.060	2	
	CCW	1000	5.0	11.00	11.74	-0.74									119										100	0.068	2	
	CCW	1000	7.5	11.00	11.88	-0.88									118										100	0.092	2	
	CCW	1000	10.0	11.00	11.97	-0.97									118										100	0.127	2	
	COW	1000	10.0	12.63	b 10.00	b 2.63	b 1.71																		100	—	—	
	COW	1000	10.0	11.00	11.88	-0.88																			100	—	—	
	CCW	1000	12.5	11.00	12.02	-1.02																			100	0.168	2	
	CCW	1000	15.0	11.00	12.11	-1.11																			100	0.180	2	
	COW	1000	20.0	11.00	12.22	-1.22																			100	0.210	2	
	CCW	1000	30.0	11.00	12.59	-1.59																		100	0.268	2		
	COW	30.0	30.0	13.01	b 11.00	b 2.01	b 1.71																	100	—	—		
	COW	30.0	30.0	11.00	12.53	-1.53																		100	—	—		
	CCW	30.0	45.0	11.00	12.93	-1.93																		100	0.320	2		
	CCW	60.0	60.0	11.00	13.35	-2.35																		100	0.350	2		
	CW	1000	3.0	13.12	11.00	2.12		112	123	123	123	123	123	109	120	122	123	122	122	122	113	80	80	SAE 10	130	100	0.045	2
	CW	1000	5.0	13.12	11.00	2.12																		100	0.071	2		
	CW	1000	7.5	13.02	11.00	2.02																		100	0.095	2		
	CW	1000	10.0	12.97	11.00	1.97																		100	0.122	2		
	CW	1000	10.0	15.45	b 10.00	b 5.45	b 1.71																	100	—	—		
	CW	1000	10.0	12.00	• 13.53	— 1.53	— 1.71																	100	—	—		
	CW	1000	10.0	13.00	11.00	2.00																		100	—	—		
	CW	1000	12.5	13.00	11.00	2.00																		100	0.160	2		
	CW	1000	15.0	12.95	11.00	1.95																		100	0.172	2		
	CW	1000	20.0	12.88	11.00	1.88																		100	0.207	2		
	CW	1000	30.0	12.78	11.00	1.78																		100	0.285	2		
	CW	1000	30.0	15.28	b 10.00	b 5.26	b 1.71																	100	—	—		
	CW	1000	30.0	12.00	• 13.83	— 1.83	— 1.71																	100	—	—		
	CW	1000	30.0	12.72	11.00	1.72																		100	—	—		
	CW	1000	45.0	12.55	11.00	1.55																		100	0.302	2		
	CW	1000	60.0	12.36	11.00	1.36																		100	0.335	2		

\* CCW, counterclockwise; CW, clockwise.

b At front of bearing hub.

c At rear of bearing hub.

TABLE III.—SAMPLE CALCULATION SHEET FOR JOURNAL DISPLACEMENTS USING SHAFT WITH TWO JOURNALS AND

SAE 10 OIL WITH  $\frac{l}{d} = \frac{1}{2}$ ,  $N = 5,000$  RPM, AND  $p_o = 100$  POUNDS PER SQUARE INCH

[Nominal bearing dimensions:  $d = 1\frac{3}{8}$  in.,  $l = 1\frac{1}{4}$  in., and  $c_d = 0.00232$  in. True bearing dimensions:  $d = 1.387$  in.,  $l = 0.688$  in.,  $\frac{l}{d} = 0.496$ ,  $(\frac{l}{d})^2 = 0.246$ ,  $(T_1 T_4 T_5)_4 = T_3 = 9.5^\circ$  F,  $c_d = 0.002025$  in.,  $(\frac{d}{c_d}) = 0.633 \times 10^4$ ,  $(\frac{d}{c_d})^2 = 0.465 \times 10^6$ , and  $N' = 83.33$  rps.]

Shaft rotation (*)	Capsule pressure, $p_c$ , lb/sq in.	Load, $P$ , lb	Bearing pressure, $p'$ , lb/sq in.	Inlet pressure, $P_{in}$ , lb/sq in.	Rider displacements, in.									
					Left vertical			Left horizontal			Right vertical			
					Load increasing	Load decreasing	Average	Load increasing	Load decreasing	Average	Load increasing	Load decreasing	Average	Load increasing
COW	4.5	0	0	4	0	$-0.40 \times 10^{-4}$	0	$-0.40 \times 10^{-4}$	0	$-0.05 \times 10^{-4}$	0	0	0	$-0.15 \times 10^{-4}$
COW	4.5	0	0	100	$-0.40 \times 10^{-4}$	$-0.40 \times 10^{-4}$	0	0.85	0.85	$0.90 \times 10^{-4}$	$0.30 \times 10^{-4}$	$0.30 \times 10^{-4}$	$0.30 \times 10^{-4}$	1.15
CCW	7.5	45.0	23.6	100	0.70	0.80	0.85	1.75	1.65	1.70	0.70	0.20	0.45	3.05
CCW	10.0	82.5	43.1	100	2.10	2.10	2.10	2.35	2.35	2.35	1.60	1.50	1.55	4.35
CCW	12.5	120.0	62.9	100	2.90	2.80	2.85	2.55	2.55	2.55	2.90	2.80	2.85	4.75
CCW	15.0	167.5	82.5	100	3.90	3.80	3.85	2.75	2.75	2.75	3.70	3.60	3.65	4.75
CCW	20.0	232.5	122.0	100	5.40	5.30	5.35	2.45	2.45	2.45	4.90	4.80	4.85	4.75
CCW	25.0	307.5	161.0	100	6.20	6.60	6.40	2.45	2.45	2.45	5.90	5.80	5.85	4.75
CCW	30.0	382.5	200.0	100	7.00	7.40	7.20	2.65	2.65	2.65	6.90	6.70	6.80	4.75
CCW	40.0	532.5	279.0	100	8.40	8.80	8.45	2.55	2.55	2.55	8.10	7.90	8.00	4.55
CCW	50.0	675.0	354.0	100	9.20	9.50	9.35	2.15	2.15	2.15	9.20	9.00	9.10	4.25
CCW	60.0	832.5	435.0	100	10.05	-----	10.05	2.10	2.10	2.10	10.00	-----	10.00	4.05
CW	4.5	0	0	4	0	0	0	0.05	-0.05	0	0.05	-0.05	0	0.35
CW	4.5	0	0	100	-0.30	-0.40	-0.35	-0.75	-1.25	-1.00	0.35	0.25	0.30	-1.45
CW	7.5	45.0	23.0	100	0.70	0.80	0.75	-2.05	-2.25	-2.15	0.15	0.25	0.20	-2.05
CW	10.0	82.5	43.1	100	1.30	2.20	1.75	-2.95	-3.35	-3.15	0.55	0.55	0.55	-4.45
CW	12.5	120.0	62.9	100	3.80	3.40	3.50	-3.85	-3.85	-3.80	1.65	1.55	1.55	-5.35
CW	15.0	167.5	82.5	100	4.20	4.10	4.15	-3.75	-4.05	-3.90	2.85	2.75	2.80	-5.55
CW	20.0	232.5	122.0	100	5.70	5.90	5.80	-4.15	-4.05	-4.10	4.25	4.35	4.30	-5.55
CW	25.0	307.5	161.0	100	6.90	6.90	6.90	-4.15	-4.05	-4.10	5.55	5.45	5.50	-5.65
CW	30.0	382.5	200.0	100	7.70	7.60	7.65	-4.05	-3.85	-3.95	6.05	6.05	6.05	-5.35
CW	40.0	532.5	279.0	100	8.90	8.70	8.80	-3.65	-3.75	-3.70	7.25	7.05	7.15	-4.85
CW	50.0	675.0	354.0	100	10.10	9.80	10.00	-3.45	-3.45	-3.45	8.25	7.85	8.05	-4.65
CW	60.0	832.5	435.0	100	10.75	-----	10.75	-3.40	-----	8.70	-----	8.70	-----	-4.15

Rider displacement, in.—Continued						Correc- tion for shaft deflection, $\delta$ , in.	Journal displacement at bearing center line, in.			Eccentricity ratio			Bearing temper- ature, $(T_1 T_4 T_5)_4$ , °F	Oil vis- cosity, $\mu$ , centipoises	Capacity number, $C_a$	Load number, $\frac{1}{C_a}$
Right horizontal—Con.		Average of left and right		Average of CW and CCW			Vertical, $\epsilon_v$	Horizon- tal, $\epsilon_h$	Verti- cal, $n_v$	Horiz- ontal, $n_h$	Radial, $n_r$					
Load decreasing	Average	Vertical	Horizontal	Vertical	Horizontal											
$0.15 \times 10^{-4}$	0	0	0	0	0	0	0	0	0	0	159	8.8	$1.275 \times 10^{-4}$	0	0	
1.45	$1.30 \times 10^{-4}$	$-0.05 \times 10^{-4}$	$1.10 \times 10^{-4}$	$-0.04 \times 10^{-4}$	$1.21 \times 10^{-4}$	0	$-0.04 \times 10^{-4}$	$1.21 \times 10^{-4}$	$-0.004$	0.119	159	8.8	1.275	0	0	
3.05	0.55	2.38	0.51	2.54	0.09 $\times 10^{-4}$	0.42	0.42	0.42	0.0415	0.250	158	8.9	1.29	0.5200	1.93	
4.45	4.40	1.83	3.38	1.49	3.66	0.17	1.32	3.66	0.132	0.360	157	9.0	1.305	0.2880	3.47	
4.75	4.75	2.85	3.65	2.69	4.15	0.21	2.48	4.15	0.244	0.410	156.5	9.1	1.32	0.2000	5.00	
4.75	4.75	3.75	3.70	3.61	4.24	0.27	3.34	4.24	0.329	0.417	156.5	9.1	1.32	0.1530	6.63	
4.75	4.75	5.10	3.68	5.07	4.28	0.40	4.67	4.28	0.400	0.421	156.5	9.1	1.32	0.1030	7.70	
4.75	4.75	6.13	3.68	6.16	4.26	0.63	5.63	4.26	0.555	0.420	156.5	9.1	1.32	0.0772	12.94	
4.75	4.75	7.00	3.65	6.92	4.16	0.68	6.26	4.16	0.616	0.410	157	9.0	1.305	0.0621	16.10	
4.45	4.50	8.23	3.43	8.10	3.89	0.91	7.19	3.89	0.708	0.383	157.5	9.0	1.305	0.0446	22.47	
4.15	4.20	9.23	3.23	9.13	3.60	1.17	7.96	3.60	0.785	0.365	158.5	8.9	1.29	0.0347	28.80	
4.05	4.05	10.03	3.03	9.88	3.43	1.43	8.45	3.43	0.833	0.338	159.5	8.8	1.275	0.0279	35.82	
$-0.35$	0	0	0	0	0	0	0	0	0	0	159	8.8	1.275	0	0	
-1.85	-1.65	-0.03	-1.33	-1.34	-0.03	-0.03	-0.03	-0.03	-0.004	0.119	159	8.8	1.275	0	0	
-3.65	-3.24	0.48	-2.70	-2.70	-0.48	-0.48	-0.48	-0.48	-0.0415	0.250	158	8.9	1.29	0.5200	1.93	
-5.05	-4.75	1.16	-3.95	-3.95	-0.51	-0.51	-0.51	-0.51	-0.132	0.360	157	9.0	1.305	0.2880	3.47	
-5.65	-5.50	2.53	-4.65	-4.65	-0.55	-0.55	-0.55	-0.55	-0.334	0.384	157	9.0	1.305	0.2880	3.47	
-5.75	-5.65	3.48	-4.78	-4.78	-0.65	-0.65	-0.65	-0.65	-0.477	0.477	156.5	9.1	1.32	0.2000	5.00	
-5.75	-5.65	5.05	-4.88	-4.88	-0.65	-0.65	-0.65	-0.65	-0.65	0.65	156.5	9.1	1.32	0.1530	6.63	
-5.05	-5.60	6.20	-4.85	-4.85	-0.60	-0.60	-0.60	-0.60	-0.60	0.60	156.5	9.1	1.32	0.1030	7.70	
-5.05	-5.40	6.85	-4.68	-4.68	-0.50	-0.50	-0.50	-0.50	-0.50	0.50	156.5	9.1	1.32	0.0772	12.94	
-5.05	-5.00	7.98	-4.35	-4.35	-0.50	-0.50	-0.50	-0.50	-0.50	0.50	157	9.0	1.305	0.0621	16.10	
-5.45	-4.50	9.03	-3.98	-3.98	-0.45	-0.45	-0.45	-0.45	-0.45	0.45	157.5	9.0	1.29	0.0347	28.80	
-5.45	-4.15	9.73	-3.78	-3.78	-0.45	-0.45	-0.45	-0.45	-0.45	0.45	159.5	8.8	1.275	0.0279	35.82	

\* CCW, counterclockwise; CW, clockwise.  
b Area of loading piston = 15.02 sq in.  $P = 15.02(p_c - 4.5)$ .  
c  $P = \frac{P}{2d}$ .  
 $\mu = \frac{Z}{6.9 \times 10^3}$ .  
d Dial readings from log sheet reduced to zero value at condition of zero load and inlet oil pressure of 4 lb/sq in. Journal is assumed to be in center of bearing at this condition.

TABLE IV.—SAMPLE CALCULATION SHEET FOR FRICTION AND OIL FLOW USING SAE 10 OIL WITH  $l/d=1$ ,  $N=1,000$  RPM, AND  $p_0=100$  POUNDS PER SQUARE INCH

[Nominal bearing dimensions:  $d=1\frac{3}{8}$  in.,  $l=1\frac{3}{8}$  in.,  $\frac{l}{d}=1$ , and  $c_d=0.00264$  in. True bearing dimensions:  $d=1.387$  in.,  $l=1.375$  in.,  $\frac{l}{d}=0.99$ ,  $\left(\frac{l}{d}\right)^2=0.98$ ,  $(T_f-T_b)=4^\circ$  F,  $c_d=0.00251$  in.,  $\frac{d}{c_d}=0.551 \times 10^3$ ,  $\left(\frac{d}{c_d}\right)^2=0.303 \times 10^4$ ,  $N=16.67$  rps, sp. gr. of oil=0.855, and  $F_e=0.485$  in-lb/in. of Hg]

Capsule pressure, $p_0$ , lb/sq. in.	$p_0-3.5$ , lb/sq. in.	Load, $P$ , lb	Bearing pressure, $p'$ , lb/sq. in.	Average manometer difference, $\Delta H_g$ , in. of Hg	Average frictional torque, $M_f$ , in-lb	Friction variable, $f_f$	Friction ratio, $F/F_e$	Bearing temperature, $T_b$ , °F	Oil viscosity, $Z$ , centipoles	Oil viscosity, $\mu$ , reyns	Capacity number, $C_a$	Load number, $1/C_a$	Average oil flow, $Q_e$ , lb	Oil flow time, min	Oil flow, $Q'$ , lb/min	Oil flow, $Q$ , cu in./sec	Oil flow number, $Q_a$
3.5	0	0	0	1.43	0.689	∞	1.130	122	17.5	$2.54 \times 10^{-6}$	0	0.0620	2.0	0.0310	0.0168	0.134	
5.0	1.5	22.5	11.8	1.43	0.694	24.10	1.138	122	17.5	2.54	1.066	0.94	0.0695	2.0	0.0348	0.0188	0.150
7.5	4.0	60.1	31.5	1.45	0.703	9.13	1.183	122	17.5	2.54	0.400	2.50	0.0935	2.0	0.0468	0.0252	0.201
10.0	6.5	97.6	51.2	1.47	0.713	5.70	1.171	122	17.5	2.54	0.246	4.06	0.1245	2.0	0.0623	0.0336	0.208
12.5	9.0	135.1	70.7	1.51	0.732	4.23	1.201	122	17.5	2.54	0.178	5.61	0.1640	2.0	0.0770	0.0415	0.330
15.0	11.5	172.6	90.5	1.53	0.742	3.36	1.219	122	17.5	2.54	0.139	7.19	0.1760	2.0	0.0880	0.0476	0.378
20.0	16.5	248.0	130.0	1.55	0.751	2.36	1.310	124	16.5	2.39	0.091	11.00	0.2115	2.0	0.1058	0.0570	0.454
30.0	26.5	398.0	208.5	1.63	0.791	1.55	1.379	124	16.5	2.39	0.0566	17.66	0.2615	2.0	0.1308	0.0705	0.561
45.0	41.5	623.0	326.5	1.74	0.844	1.06	1.470	124	16.5	2.39	0.0363	27.55	0.3110	2.0	0.1555	0.0840	0.670
60.0	56.5	848.0	446.0	1.855	0.899	0.83	1.617	126	16.0	2.32	0.0268	33.80	0.3425	2.0	0.1713	0.0925	0.736

\* Area of loading piston=15.02 sq in.  $P=15.02 (p_0-3.5)$ .

b  $p' = \frac{P}{ld}$ .

c  $M_f = F_e \times \Delta H_g$ .

d  $f_f = f \left( \frac{d}{c_d} \right) \left( \frac{l}{d} \right)^2$   
 $\frac{M_f}{P r} \left( \frac{d}{c_d} \right) \left( \frac{l}{d} \right)^2$

e  $\frac{F}{F_e} = \frac{M_f d r}{2 \pi^2 \mu d N^2} \left( \frac{d}{c_d} \right)$

$\mu = \frac{Z}{6.9 \times 10^6}$

$Q = Q' \times \frac{1728}{62.4 \times 0.855} \times \frac{1}{60}$

$= 0.54 Q'$

f  $Q_a = \frac{2Q}{\pi d l c_d N^2}$

$= 7.97 Q$

$= 7.97 Q$